RESEARCH ARTICLE

MICROBIOLOGY

Electrochemical potential enables dormant spores to integrate environmental signals

Kaito Kikuchi[1]†, Leticia Galera-Laporta[1]†, Colleen Weatherwax[1], Jamie Y. Lam[2], Eun Chae Moon[1], Emmanuel A. Theodorakis[2], Jordi Garcia-Ojalvo[3], Gürol M. Süel[1,4,5]*

The dormant state of bacterial spores is generally thought to be devoid of biological activity. We show that despite continued dormancy, spores can integrate environmental signals over time through a preexisting electrochemical potential. Specifically, we studied thousands of individual *Bacillus subtilis* spores that remain dormant when exposed to transient nutrient pulses. Guided by a mathematical model of bacterial electrophysiology, we modulated the decision to exit dormancy by genetically and chemically targeting potassium ion flux. We confirmed that short nutrient pulses result in step-like changes in the electrochemical potential of persistent spores. During dormancy, spores thus gradually release their stored electrochemical potential to integrate extracellular information over time. These findings reveal a decision-making mechanism that operates in physiologically inactive cells.

The formation of bacterial spores (sporulation) is a common and well-characterized survival strategy in many microbial species (*1*, *2*). Spores are partially dehydrated cells enclosed by a protective coat that can survive environmental extremes and remain dormant for years (*3*). They need to be robust to environmental fluctuations to avoid exiting their dormant state (germinating) prematurely. At the same time, spores need to germinate if they detect favorable conditions (*4*) (Fig. 1A). Germination requires the rehydration of the spore, which is promoted by the release of calcium-dipicolinic acid (CaDPA) (*5*). Aside from degradation of RNA immediately after sporulation (*6*), dormant spores appear to have no measurable metabolic or biological activity (*7*). Therefore, it remains unclear whether dormant spores possess any activity that could affect the choice of whether or not to germinate. We thus tested whether dormant *Bacillus subtilis* spores experience any physiological changes in response to subtle environmental signals that do not trigger germination. Addressing these questions could reveal how spores reconcile their robust dormant state with the need to process extracellular information and make an informed decision on whether to continue or exit their dormancy.

Spores can be pretreated with nutrients to promote germination (*8*–*10*). These findings imply that spores can somehow integrate extracellular signals despite their dormancy and thereby alter their future likelihood of triggering germination. Although there are no well-established mechanisms for dormant cells to integrate extracellular information, the ability of spores to modulate their future response suggests a conceptual similarity to a decision-making mechanism in neuroscience known as integrate-and-fire (*11*, *12*). This mechanism describes how neurons respond to small synaptic inputs before reaching the threshold that triggers an action potential (*13*). It is unclear whether dormant spores use a similar mechanism to process environmental inputs and modulate their approach toward a threshold that triggers germination.

Given the physiological inactivity of spores, we investigated a possible integration mechanism based on passive ion flux, which does not require cellular energy. Our findings indicate that physiologically inactive spores integrate environmental signals by modifying preexisting ion gradients that were established during sporulation. Dormant spores can thus use stored electrochemical potential energy to regulate their cell-fate decision without requiring de novo adenosine triphosphate (ATP) synthesis. In this way, spores can alter their distance to the germination threshold depending on environmental inputs while still in the dormant state. This mechanism also reconciles the robust dormancy of spores with the ability to gradually become sensitized to future environmental signals.

Results

B. subtilis *spores can remain dormant despite exposure to germinant pulses*

We confirmed that similar to laboratory strains, undomesticated *B. subtilis* spores can be pretreated with short nutrient (germinant) pulses to increase the likelihood of germination (*8*). Specifically, we imaged spores (Fig. 1B) within a microfluidic device that allows single-cell monitoring and precise control over the components in the incubation medium (materials and methods). We optically tracked the switch in phase-contrast brightness that results from the rehydration of spores during germination (*4*, *14*) (Fig. 1C and fig. S1, A and B). Using this experimental approach, we exposed thousands of spores to a single short germinant pulse [10 mM L-alanine for 3 min] and found that ~95% of spores remained dormant (95.2% ± 1.9%, n = 2244) (Fig. 1D). We used the germinant L-alanine because it is a naturally occurring nutrient that triggers germination through designated receptors in bacterial spores (*15*). Spores that did not germinate upon stimulation remained dormant for at least the next 20 hours of imaging (fig. S1C). Any spore that did germinate in response to the germinant pulse did so on average within 15 min (14.85 ± 1.07, n = 1831) (fig. S1D).

To quantify the integration capacity of spores, we applied a second germinant pulse, which was separated by 2 hours from the first pulse to ensure that germination in response to the first pulse of germinant had subsided. After the second pulse, approximately half of the remaining spores germinated (52.1% ± 6.2%). The germination propensity of spores was independent of their location within the microfluidic chamber (fig. S2). We defined the spore's integration capacity as the population-level change (difference) in the germination probability in response to two consecutive germinant pulses (Fig. 1E). The germination probability increased by 47% ± 1% (mean ± SD, n = 9 replicate populations) between the first and second pulse. Spores thus become sensitized by the first exposure and appear to move closer toward a germination threshold.

A mathematical model of the role of ion flux in responding to germinant pulses

To explain how physiologically inactive spores could integrate information about germinant exposure over time, we explored an ion flux as a mechanism, as this process could occur passively with preexisting ionic gradients established during sporulation. Other processes such as de novo gene expression and enzymatic activity typically require energy, which is highly limited in spores. In particular, we focused here on the flux of potassium because it is the most abundant intracellular ion in bacteria and has physiological roles in the stress response of *B. subtilis* (*16*–*19*). Furthermore, potassium ions have been proposed to stabilize the formation of bacterial spores (*20*). To investigate the possible role of potassium ion flux in dormant spores, we developed a mathematical model based on the Hodgkin–Huxley framework

[1]Molecular Biology Section, Division of Biological Sciences, University of California San Diego, La Jolla, CA 92093, USA. [2]Department of Chemistry and Biochemistry, University of California San Diego, La Jolla, CA 92093, USA. [3]Department of Medicine and Life Sciences, Universitat Pompeu Fabra, 08003 Barcelona, Spain. [4]UCSD Synthetic Biology Institute, University of California San Diego, La Jolla, CA 92093, USA. [5]Center for Microbiome Innovation, University of California San Diego, La Jolla, CA 92093, USA.
*Corresponding author. Email: gsuel@ucsd.edu
†These authors contributed equally to this work.

Downloaded from https://www.science.org at University of California San Diego on October 06, 2022

(*21*) (Fig. 1F, Box 1, and supplementary text). Our model describes how potassium ion flux can drive a spore toward a fixed germination threshold through an integrate-and-fire mechanism, without requiring any physiological activity.

Our mathematical model assumes that potassium ions enter or leave a spore through passive transport through both selective potassium channels and nonspecific ion channels. The direction and rate of potassium flux across the spore membrane depend on the potassium ion concentration gradient, as well as on the membrane potential of the spore (*16*–*19*) (supplementary text). Spores contain high amounts of potassium (*22*, *23*), which would result in ion efflux when channels are open. We assume that ion pumps are inactive during dormancy, given that they require ATP for transport, which is highly limited and not actively produced in spores (*6*). Furthermore, the model assumes that ion channels (both potassium specific and nonspecific) are closed until germinant is added. The channels open in the presence of germinant and close in its absence. Lastly, we assume that the initial potassium content of spores has some variability and that germination begins when a spore's internal potassium concentration drops below a certain value (that is, it reaches the germination threshold) (Fig. 1, G and H). Given these assumptions, the model predicts that, when exposed to consecutive short germinant pulses, few spores germinate during the first pulse, whereas most spores do so during the second or subsequent pulses (Fig. 1I). This increase in the germination probability of spores is consistent with our experimental observations (Fig. 1D). Different germinant concentrations in the first pulse did not markedly change the fraction of germinated spores (fig. S3). By contrast, the germinated fraction increased with higher concentration of L-alanine in the second pulse. This difference in the sensitivity of spores to the first and second germinant pulse concentrations further demonstrates integration of information. The efflux of potassium from dormant spores was also confirmed with an extracellular potassium indicator, Asante Potassium Green-4 tetramethylammonium salt (APG-4 TMA) (fig. S4, A and B). Our modeling approach thus shows how spores might use intracellular potassium concentration to integrate information about previous germinant exposures and change their sensitivity to future exposures.

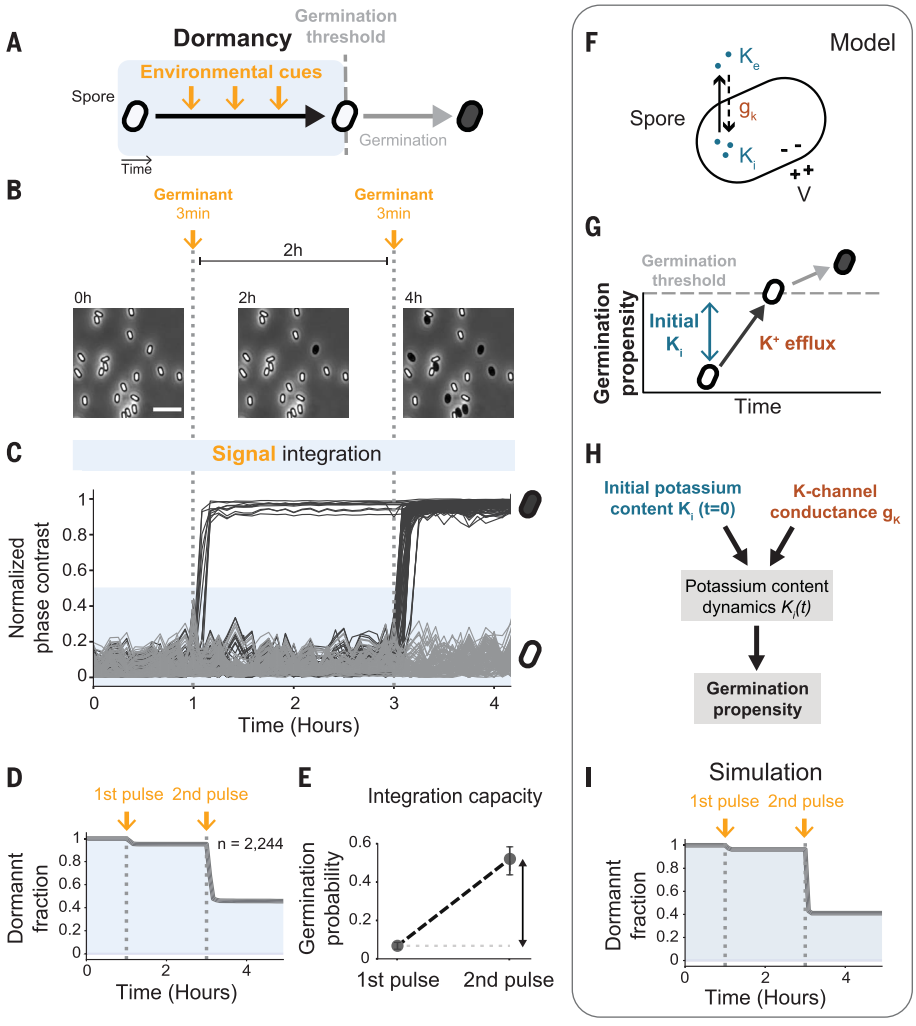

Fig. 1. *B. subtilis* spores integrate over two consecutive germinant pulses. (**A**) Bacterial spores can remain in dormancy (shaded area in blue) for years seemingly without any biological activity. It is thus unclear how spores sense environmental cues while dormant and before triggering germination. (**B**) Filmstrip from phase-contrast microscopy that shows the fractional germination response to the pulses. Spores contained in a microfluidic chip were subjected to 3-min germinant pulses (10 mM L-alanine, dotted vertical lines) separated by 2-hour intervals. These pulses triggered germination of a subset of spores, which was detected by phase-contrast imaging: White dormant spores become phase dark when germinating as they rehydrate. Spores that maintain dormancy despite exposure to germinant pulses provoke the question of whether they can sense and process such environmental information. Scale bar, 5 μm. (**C**) Single-cell time traces showing the change in the normalized phase-contrast intensity during spore germination [n = 200, subset of data from (D)]. Collective fluctuations in the image intensity are due to subtle changes in camera focus. (**D**) Fraction of dormant spores after each germinant pulse (n = 2244). The abrupt decrease in the dormant fraction after the second germinant pulse indicates the ability of spores to integrate signals over consecutive pulses. (**E**) The germination probability in each pulse is calculated based on the remaining dormant spores before each germinant pulse. The difference in the germination probability between the two pulses (vertical arrow) provides a metric to quantify the information integration by spores. (**F**) Cartoon showing the main components of our mathematical model. The flux of potassium in a spore is assumed to depend partially on the difference between its internal (K_i) and external (K_e) concentrations, the K-channel conductance (g_K), and the membrane potential (V) of the spore. (**G**) Spore's approach to the germination threshold is dictated by initial potassium content (K_i) and potassium efflux. (**H**) In the mathematical model, the initial potassium content (K_i, t = 0) and the K-channel conductance (g_K) determine the potassium dynamics in spores [$K_i(t)$]. These dynamics determine the spore's propensity to germinate (see Box 1 and supplementary text). (**I**) Simulated fraction of dormant spores after each germinant pulse.

Initial potassium concentrations define the distance to the germination threshold

Our mathematical model assumes that the initial potassium content defines the distance to the germination threshold (Fig. 1, G and H). To test this, we generated a mutant strain in which the KtrC subunit of the KtrCD potassium importer was deleted, which is expected to lower intracellular potassium content and, consequently, put the spore closer to the threshold compared with wild-type spores (Fig. 2A). KtrC is the major potassium importer expressed in the inner spore membrane during the sporulation process (*24*), which enables potassium uptake (*25*, *26*) (Fig. 2, B and C). By generating spores in the presence of an intracellular potassium indicator, APG-4 acetoxymethyl ester

Downloaded from https://www.science.org at University of California San Diego on October 06, 2022

(AM), we confirmed that the Δ*ktrC* spores contain less potassium than do wild-type spores (fig. S4, C through F). Accordingly, the Δ*ktrC* spores are mathematically predicted to be more likely to germinate in response to the first germinant pulse (Fig. 2D). Indeed, measurements show that 42% of the Δ*ktrC* spores germinated after the first pulse, compared with 5% of the wild-type spores (Fig. 2, E through G, and movie S1). The germinated fraction of Δ*ktrC* spores then further increased after the second pulse (Fig. 2H). We obtained similar results with spores that lacked KtrD, the other subunit of the KtrCD potassium importer (fig. S5A).

Given the high germination probability of Δ*ktrC* spores, almost the entire population (~94%) exited the dormant state after only two germinant pulses (Fig. 2G). However, because the deletion of *ktrC* does not affect potassium efflux in spores, the integration capacity of Δ*ktrC* spores is comparable to that of wild-type spores (Fig. 2I). To further confirm that the lower potassium content of Δ*ktrC* spores caused the higher sensitivity to germinant pulses, we supplied additional potassium during the sporulation of Δ*ktrC* cells. Increasing the potassium content in Δ*ktrC* spores should increase their distance to the germination threshold, which in turn would be reflected in a decrease in their germination probability (fig. S5B). In agreement with those expectations, the addition of 150 mM of potassium in the sporulation medium resulted in Δ*ktrC* spores that responded to germinant pulses similarly to wild-type spores (fig. S5, C and D). These results are consistent with the modeling prediction and support the idea that the initial intracellular potassium concentration of spores specifically defines their distance to the germination threshold.

Potassium ion channels contribute to the integration capacity of spores

We investigated the modeling prediction that spores use potassium efflux to integrate over consecutive germinant pulses. To this end, we studied a mutant strain lacking the YugO potassium ion channel (*27*) (Fig. 3, A and B). We confirmed that Δ*yugO* spores contain less potassium than do wild-type spores with the intracellular potassium indicator APG-4 AM (fig. S4, C through F). Therefore, the Δ*yugO* spores should be initially closer to the germination threshold and be more sensitive than wild-type spores to the first germinant pulse (Fig. 3, A through D). However, the absence of the YugO channel also implies a reduced potassium efflux in response to germinant pulses. According to our model, such reduced potassium efflux in germinant-exposed spores should lower their integration capacity, and thus, the germination probability for subsequent germinant pulses would be lower (Fig. 3D). In other words, the Δ*yugO* spores would not markedly increase their sensitivity to consecutive germinant pulses, which should distinguish this strain from the wild-type and the Δ*ktrC* strains. These mutant spores are therefore predicted to approach the germination threshold more gradually because of reduced potassium efflux.

We experimentally tested these predictions. Essentially, the progression of the wild-type and the Δ*yugO* spores toward the germination threshold are predicted to exhibit a crossover point (Fig. 3D). Experiments confirmed that the Δ*yugO* spores have a higher response than the wild type to the first germinant pulse (with 30% versus 5% of the spores germinating, respectively) (Fig. 3, E, F, and H; movie S2). However, these spores lacked the increase in germination probability in response to subsequent pulses exhibited by the wild-type spores (Fig. 3I). This, in turn, reflects a substantial loss in integration capacity of the Δ*yugO* spores when compared with the wild type (Fig. 3J and fig. S6). The phenotype of the Δ*yugO* spores (high initial germination probability and low integration capacity) is thus consistent with our modeling predictions. Notably, the Δ*yugO* strain also indicates that the reduced efflux of potassium decreases the integration capacity of spores. These results suggest that potassium efflux serves as an integration mechanism that modulates the approach to the germination threshold.

Given the complex phenotype of the Δ*yugO* strain, we turned to chemical perturbations of potassium flux in wild-type spores to independently determine whether potassium flux underlies the integration capacity of spores. We confirmed that modifying the external potassium concentration changed the integration capacity of wild-type spores (fig. S6). Specifically, the absence of potassium in the medium, which we expected to promote higher potassium efflux in spores, increased the integration capacity (from 0.47 ± 0.01 to 0.63 ± 0.02). By contrast, increasing extracellular potassium concentration lowered the integration capacity (Media + 600 mM KCl: 0.32 ± 0.01; Media + 1 M KCl: 0.03 ± 0.01). To test whether reduction in integration capacity might result from increased osmotic stress, we showed that adding 1 M sorbitol had no effect on integration capacity (Media + 1 M sorbitol: 0.44 ± 0.02). The electrochemical gradient of potassium thus influences the integration capacity of spores.

We also tested how the integration capacity of wild-type spores is affected by blocking potassium channels with the drug quinine (1 mM) (Fig. 3, A through C, and figs. S4B and S6) (*28*–*31*). According to our model, such blocking of potassium channels is expected to specifically reduce the germination probability in response to consecutive germinant pulses (Fig. 3D). In agreement with this prediction, treatment of spores with quinine reduced the response of wild-type spores to the second germinant pulse, with around 80% of the spores remaining dormant, in comparison with around 45% in the absence of the drug (Fig. 3, G, H, and I; movie S3). These results support the proposed integrate-and-fire mechanism by showing that similar to the deletion of the YugO channel, chemical blocking of potassium efflux in wild-type spores also impairs their integration capacity (Fig. 3J and fig. S6).

Changes in the electrochemical potential of dormant spores

Our mathematical model proposes that the flux of potassium ions driving the processing of information during dormancy is modulated by the electrochemical potential of the spores. According to the integrate-and-fire mechanism,

Box 1. Mathematical model of dormant spore electrophysiology

According to the processes depicted in Fig. 1F, we assume that the changes in concentrations of extracellular and intracellular potassium—K_e and K_i, respectively—are governed by the flow of potassium ions through the spore membrane:

$$\frac{dK_e}{dt} = Fg_K n^4(V - V_K) + Fg_n n^4(V - V_n) - \gamma_e(K_e - K_m)$$
$$\frac{dK_i}{dt} = -Fg_K n^4(V - V_K) - Fg_n n^4(V - V_n)$$

The model includes ion flow through both specific and nonspecific channels, with conductances g_K and g_n, respectively. Additionally, extracellular potassium is subject to a relaxational term (third term in the right-hand side of the K_e equation) that pulls it to the concentration of potassium in the medium, K_m. Ion flow through the channels depends on the electrochemical state of the spore, given by its membrane potential V and reversal potentials V_K and V_n, which correspond to specific and nonspecific ions, respectively. Crucially, the reversal potential of potassium depends on the potassium concentrations through the Nernst equation:

$$V_K = V_{K0} \ln(K_e/K_i)$$

As mentioned in the main text, the channels are assumed to open in the presence of germinant, which produces an outward flux of potassium and consequently a sudden increase in membrane potential. The dynamics of the membrane potential V and gating variable n are described in the supplementary text, together with the rest of the parameters and all parameter values.

Downloaded from https://www.science.org at University of California San Diego on October 06, 2022

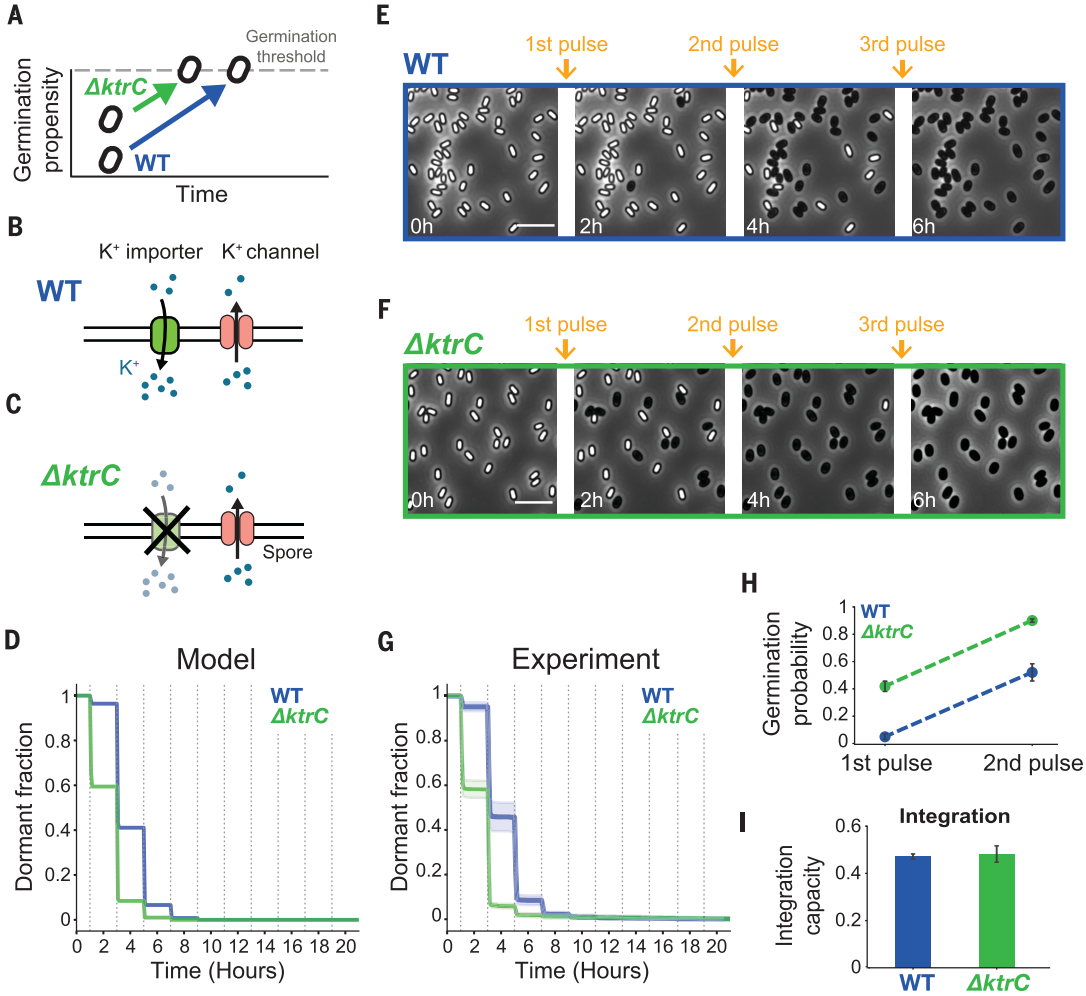

Fig. 2. Role of potassium in the germination threshold. (**A**) Model predicts that the deletion of the KtrC importer reduces the distance of spores to their germination threshold. This, in turn, will increase the germination propensity of Δ*ktrC* spores compared with wild-type (WT) spores. (**B**) WT cells contain both potassium importers and ion channels. (**C**) The *ktrC* mutant spores (Δ*ktrC*) lack the gene for the potassium importer KtrC. (**D**) Model-generated dormant fraction of the WT (blue), and the Δ*ktrC* (green) strains. Dotted vertical lines indicate germinant pulses. (**E** and **F**) Phase-contrast microscopy filmstrips for representative WT (E) and Δ*ktrC* spores (F), respectively. Snapshots show spores before and after the indicated germinant pulses. Scale bars, 5 μm. (**G**) Dormant fraction from single-cell experimental results for WT (blue, mean ± SD, n = 2244, data from Fig. 1D) and Δ*ktrC* (green, mean ± SD, n = 2154). Dotted vertical lines indicate germinant pulses. (**H**) Germination probabilities of the WT and the Δ*ktrC* spores increase with consecutive pulses. Both strains reach 50% germination out of all initial spores (half-maximum germination) after two consecutive pulses. Error bars represent standard deviation. (**I**) Bar plot showing the integration capacity of the WT and the Δ*ktrC* strains (0.47 ± 0.01 and 0.48 ± 0.03, respectively) calculated from the differences in germination probabilities shown in (H). Error bars represent standard deviation.

spores that are further from their germination threshold would require multiple germinant pulses to reach the threshold, each pulse causing an incremental electrochemical potential change (Fig. 4A). Specifically, the transient efflux of potassium cations triggered by germinant pulses is mathematically predicted to increase the negative electrochemical potential of spores in a step-like manner, even when the pulses do not trigger germination (Fig. 4B). To test this prediction, we used a previously characterized cationic fluorescent dye, thioflavin-T (ThT) to measure changes in the electrochemical potential of dormant spores (materials and methods) (*16*, *32*). As spores are notoriously impermeable to most chemicals (*33*), we expected that peripheral staining by ThT would reflect the spore's overall negative electrochemical potential (*20*).

To experimentally test our modeling prediction of electrochemical potential jumps, we tracked thousands of individual wild-type spores over time and simultaneously imaged phase-contrast and ThT fluorescence intensities (Fig. 4, C through F). Spores that did not trigger germination exhibited sudden changes in their electrochemical potential in response to germinant pulses (movie S4). Spores that required multiple germinant pulses to trigger germination exhibited a multistep progression before reaching their germination threshold. These increases in the ThT signal were not due to increased spore permeability, as ThT continued to stain the spore's periphery and did not transition to its interior (Fig. 4D and movie S4). Therefore, accumulation of ThT on the spore periphery appears to reflect changes in the ionic content of the spore. We observed no characteristic changes of the phase-contrast brightness of dormant spores during the increases in the ThT signal (fig. S7A). We also tested L-valine, another naturally occurring germinant (*34*), and observed similar changes in ThT signal (fig. S7B). Furthermore, we used another positively charged dye, tetramethylrhodamine methyl ester (TMRM), which is commonly used to measure the electrochemical potential of cells (*35*). TMRM also stained the periphery of spores, and increases in the TMRM signal amplitude were qualitatively similar to those measured with ThT (fig. S8, A and B). To validate that the observed jumps in fluorescence during germinant additions were not simply a staining artifact, we synthesized a charge-neutral version of ThT (Fig. 4E, inset; figs. S8, C and D, and S9; materials and methods; and supplementary text). Although this charge-neutral ThT dye also stained the spore periphery, we observed no increases in the signal amplitude during germinant pulses. Instead, the fluorescence signal of the neutral ThT dye monotonically decayed over time, which was likely due to photobleaching. To exclude the possibility that the observed changes in electrochemical potential could be related to the release of CaDPA during the initiation of germination, we generated a mutant strain that lacked a subunit of the SpoVA channel, namely SpoVAF (fig. S10A). This subunit is

Downloaded from https://www.science.org at University of California San Diego on October 06, 2022

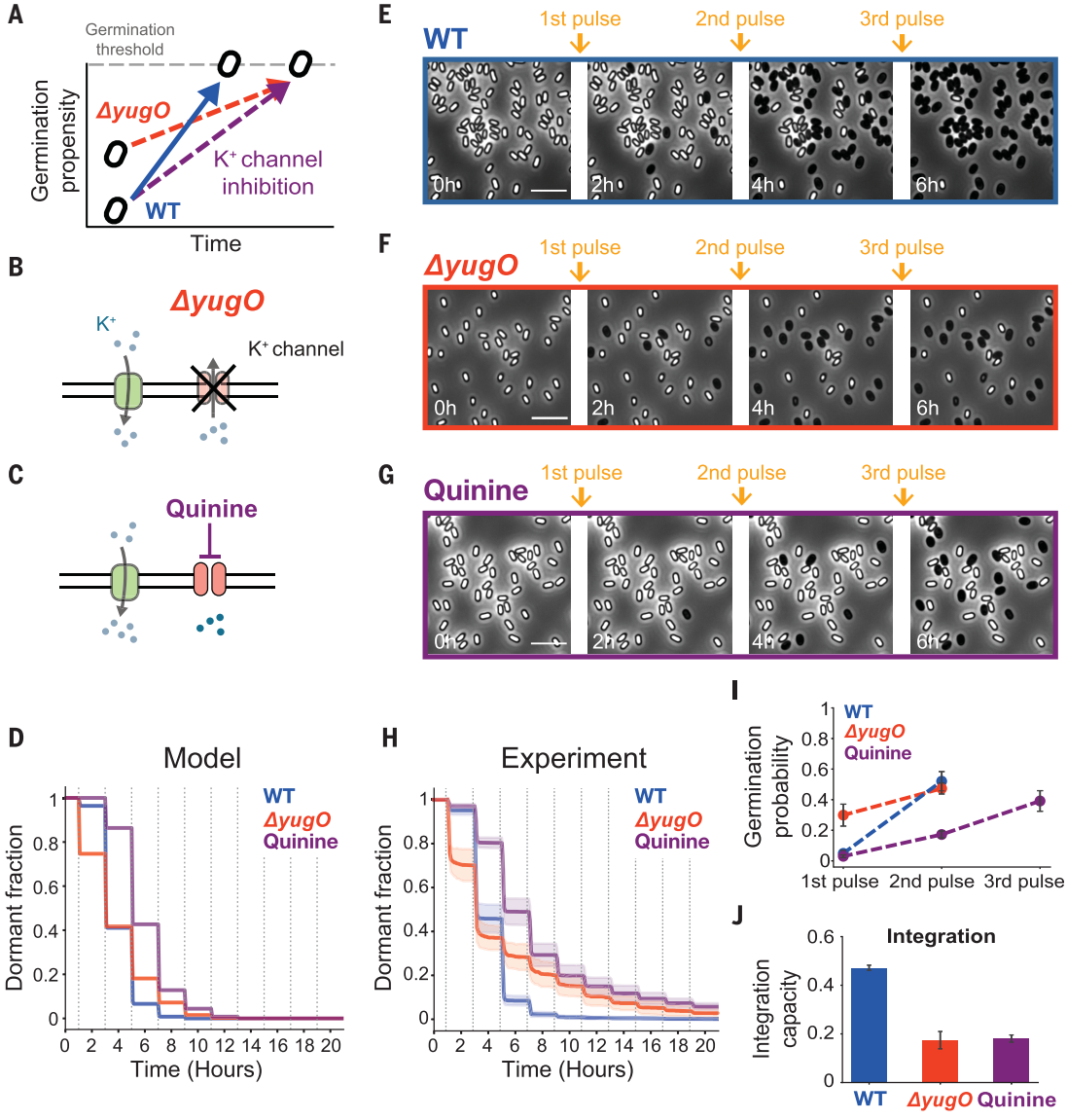

Fig. 3. Potassium ion flux underlies integration capacity of dormant spores. (**A**) Δ*yugO* mutant spores are expected to be initially closer to the germination threshold but have slower potassium efflux, which affects their approach to the threshold. The inhibition of potassium channels in WT spores is similarly expected to affect their approach to the germination threshold. (**B**) Δ*yugO* mutant spores lack the gene for the YugO channel, which is the only known potassium-specific channel in *B. subtilis* spores. (**C**) Quinine targets potassium channels, which blocks ion efflux. (**D**) Model-generated dormant fraction of WT (blue), Δ*yugO* (red), and quinine addition to WT spores (purple). (**E** to **G**) Filmstrips for representative WT (E) and Δ*yugO* (F) spores and WT spores in the presence of 1 mM quinine (G), respectively. Snapshots show spores before and after the indicated germinant pulses. Scale bars, 5 μm. (**H**) Dormant fraction from single-cell measurements of WT (mean ± SD; blue, n = 2244, data from Fig. 1D), Δ*yugO* (mean ± SD; red, n = 1058), and 1 mM quinine addition to WT spores (mean ± SD, purple, n = 4491). (**I**) Germination probability until half-maximum germination for WT (data from Fig. 2H), Δ*yugO*, and quinine addition. The inhibition of potassium efflux reduces the germination probability, requiring three pulses to reach the half-maximum germination. Error bars represent standard deviation. (**J**) Genetic and chemical inhibition of potassium efflux (Δ*yugO* and quinine addition, respectively) reduces the integration capacity of spores (WT 0.47 ± 0.01, data from Fig. 2I, Δ*yugO* 0.17 ± 0.04, and quinine 0.18 ± 0.01; mean ± SD).

essential for effective CaDPA release during germination, and its deletion causes a delay in germination (*36*). The deletion of SpoVAF slowed the response time of spores to L-alanine (fig. S10B). However, loss of *spoVAF* did not affect the electrochemical potential changes that we observed in spores (fig. S10, C and D), which indicates that CaDPA release is not required for the integration of information in dormant spores. Together, these results demonstrate that germinant pulses cause sudden changes in the electrochemical potential of spores that otherwise remain dormant. As predicted, spores that required multiple germinant pulses to initiate germination also exhibited multiple jumps in their electrochemical potential, which indicates their greater distance to the germination threshold. The ability to visualize and observe a multistep and gradual approach of dormant spores toward their germination threshold provides further evidence in support of the integrate-and-fire mechanism.

We investigated whether the integration capacity that we determined from population-level statistics correlated with the independently observed jumps in the electrochemical potential of individual spores. In particular, a higher integration capacity should correlate with a higher change in electrochemical potential. We therefore measured germinant-induced changes in the electrochemical potential for thousands of spores obtained from various perturbations considered in this study (Fig. 4, F and G). Higher integration capacity correlated with a higher average increase in electrochemical potential (Fig. 4H). Specifically, wild-type and Δ*ktrC* spores, which have similarly high changes in electrochemical potential, also exhibited relatively higher integration capacities. Furthermore, the Δ*yugO* and the quinine-exposed wild-type spores, which both exhibited lower average changes in their electrochemical potential, had reduced integration capacities. These findings support the prediction that dormant spores integrate environmental information through ion flux-induced changes in their electrochemical potential.

Discussion

We studied how physiologically inactive spores detect and respond to transient germinant pulses.

Downloaded from https://www.science.org at University of California San Diego on October 06, 2022

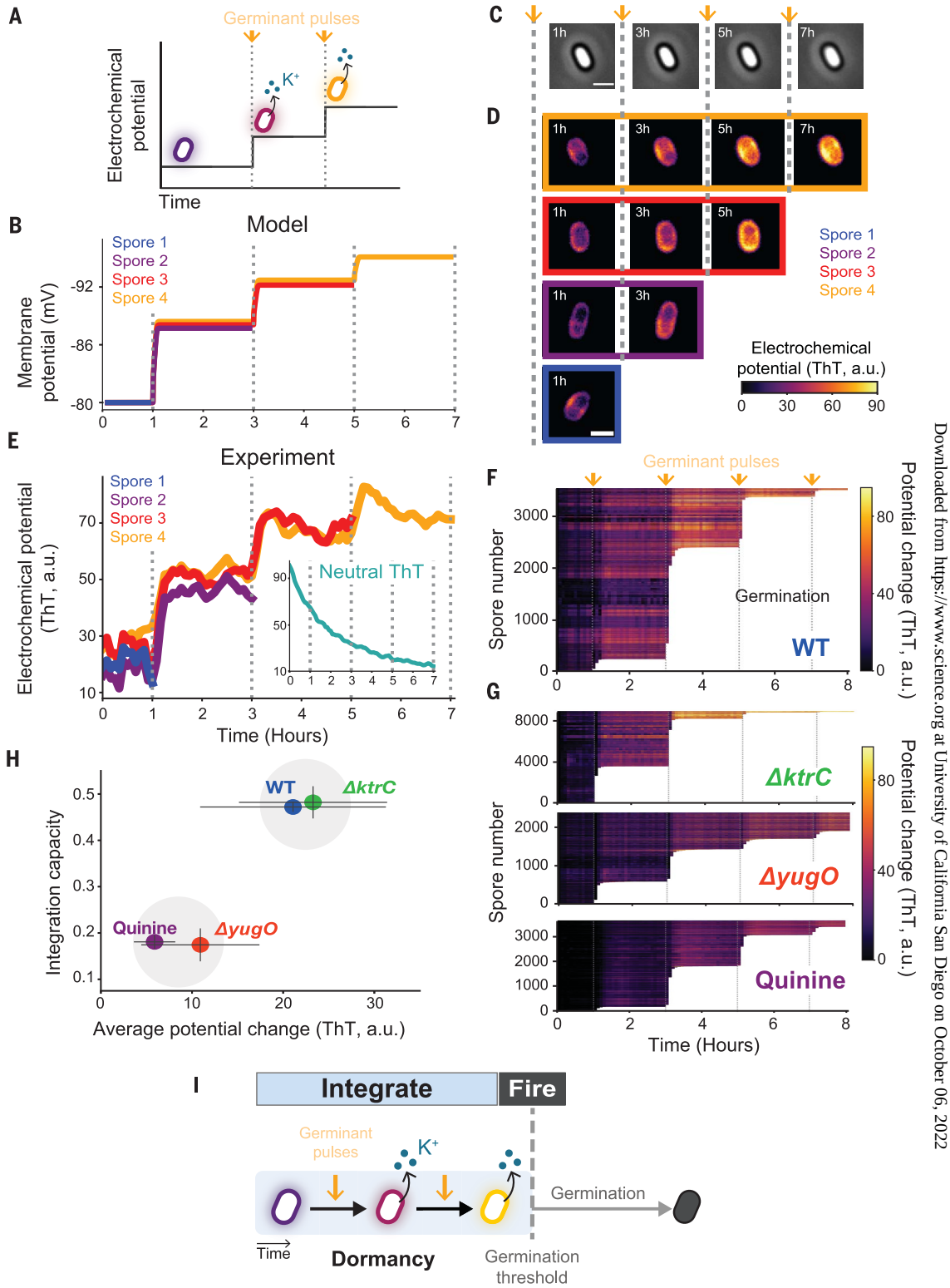

Fig. 4. Dormant spores exhibit sudden changes in their electrochemical potential, visualizing integration over germinant pulses. (**A**) Cartoon illustrating the hypothesis that spores release potassium after each germinant pulse, generating a change in their electrochemical potential. (**B**) Mathematically predicted stepwise membrane potential (mV) jumps when spores are exposed to germinant pulses (dotted vertical lines). Depicted are representative time traces for individual spores that germinate in response to different germinant pulse numbers. The termination of the time trace indicates germination. (**C**) Phase-contrast images of a spore that remains dormant (phase bright) despite exposure to three consecutive germinant pulses. Dotted vertical lines indicate germinant pulse exposure. Scale bar, 1 μm. (**D**) Top fluorescence filmstrip shows the color-coded electrochemical potential amplitude [ThT, arbitrary units (a.u.)] of the spore depicted in (C). The other three filmstrips below show individual spores, each of which germinate in response to different germinant pulses. (**E**) Single-cell time traces of the electrochemical potential signal (ThT, a.u.) for the corresponding spores in Fig. 3D (see fig. S7A for corresponding phase-contrast traces). The termination of the time traces indicates germination. The inset shows the time trace of a single spore stained with the charge-neutral ThT fluorescent dye (see fig. S8D for data from multiple spores). (**F**) Measurement of 3484 individual WT spores showing amplitude color-coded time traces that show the changes in electrochemical potential signal (ThT, a.u.) triggered by germinant pulses (dotted vertical lines). The termination of the time trace (white region) indicates germination. (**G**) Single-cell time traces of the potential change (ThT, a.u) for Δ*ktrC* (n = 8790), Δ*yugO* (n = 2380), and WT with 1 mM quinine (n = 3653), respectively. Each line represents a single-spore time trace until germination (white region). Germinant pulses are indicated with arrows and dotted vertical lines. (**H**) Scatter plot of the integration capacity as a function of the average potential change (ThT, a.u) of all strains and conditions tested in this study: WT, Δ*ktrC*, Δ*yugO*, and WT with quinine. (**I**) Conceptual summary of the proposed integrate-and-fire mechanism. Spores integrate germinant exposure information over time through efflux of potassium ions. The resulting change in electrochemical potential drives them toward a germination threshold. Spores that reach the threshold "fire" the germination program, which is marked by the abrupt change in phase-contrast refractility.

Downloaded from https://www.science.org at University of California San Diego on October 06, 2022

Our results reveal that despite their dormancy, spores can integrate extracellular information and alter their intrinsic state. This ability to process information appears to be supported by preexisting ionic gradients generated during sporulation. In this way, dormant spores can reach the decision to initiate germination by using electrochemical potential energy, rather than requiring a source of cellular energy, such as ATP. Spores may thus be analogous to a biological capacitor in that they store and use an electrochemical potential to move closer to the germination threshold (Fig. 4I). The integrate-and-fire model proposed here provides both a conceptual and mechanistic explanation for how spores can respond to an environmental signal despite being physiologically inactive. The ability to sum inputs over time before reaching a threshold ensures that germination is triggered only when favorable conditions persist while ignoring small environmental fluctuations. Although the integrate-and-fire model is used to describe how neurons process information, our work suggests that this concept may represent a more general solution to the need for information processing in diverse biological systems, including energy-limited cells.

REFERENCES AND NOTES

1. P. Stragier, R. Losick, *Annu. Rev. Genet.* **30**, 297–41 (1996).
2. P. J. Piggot, D. W. Hilbert, *Curr. Opin. Microbiol.* **7**, 579–586 (2004).
3. M. Huang, C. M. Hull, *Curr. Genet.* **63**, 831–838 (2017).
4. R. Pandey *et al*., *PLOS ONE* **8**, e58972 (2013).
5. S. Wang, P. Setlow, Y. Q. Li, *J. Bacteriol.* **197**, 1095–1103 (2015).
6. P. Setlow, G. Christie, *Front. Microbiol.* **11**, 596092 (2020).
7. S. Ghosh, G. Korza, M. Maciejewski, P. Setlow, *J. Bacteriol.* **197**, 992–1001 (2015).
8. S. Wang, J. R. Faeder, P. Setlow, Y. Q. Li, *mBio* **6**, e01859–e15 (2015).
9. P. Zhang, J. Liang, X. Yi, P. Setlow, Y. Q. Li, *J. Bacteriol.* **196**, 2443–2454 (2014).
10. L. V. Pedrero-López, B. Pérez-García, K. Mehltreter, M. E. Sánchez-Coronado, A. Orozco-Segovia, *J. Plant Physiol.* **232**, 284–290 (2019).
11. N. Brunel, M. C. W. van Rossum, *Biol. Cybern.* **97**, 337–339 (2007).
12. H. C. Tuckwell, *Introduction to Theoretical Neurobiology* (Cambridge Studies in Mathematical Biology, Cambridge University Press, 1988).
13. A. N. Burkitt, *Biol. Cybern.* **95**, 1–19 (2006).
14. P. Setlow, *J. Bacteriol.* **196**, 1297–1305 (2014).
15. A. Moir, G. Cooper, *Microbiol. Spectr.* 10.1128/microbiolspec.TBS-0014-2012, (2015).
16. A. Prindle *et al*., *Nature* **527**, 59–63 (2015).
17. J. W. Larkin *et al*., *Cell Syst.* **7**, 137–145.e3 (2018).
18. C.-Y. Yang *et al*., *Cell Syst.* **10**, 417–423.e3 (2020).
19. J. Humphries *et al*., *Cell* **168**, 200–209.e12 (2017).
20. T. Sirec, J. M. Benarroch, P. Buffard, J. Garcia-Ojalvo, M. Asally, *iScience* **16**, 378–389 (2019).
21. A. L. Hodgkin, A. F. Huxley, *J. Physiol.* **117**, 500–544 (1952).
22. E. Eisenstadt, *J. Bacteriol.* **112**, 264–267 (1972).
23. A. M. Whatmore, J. A. Chudek, R. H. Reed, *J. Gen. Microbiol.* **136**, 2527–2535 (1990).
24. L. Zheng *et al*., *J. Proteome Res.* **15**, 585–594 (2016).
25. G. Holtmann, E. P. Bakker, N. Uozumi, E. Bremer, *J. Bacteriol.* **185**, 1289–1298 (2003).
26. J. Stautz *et al*., *J. Mol. Biol.* **433**, 166968 (2021).
27. M. E. Lundberg, E. C. Becker, S. Choe, *PLOS ONE* **8**, e60993 (2013).
28. J. P. Barfield, C. H. Yeung, T. G. Cooper, *Mol. Hum. Reprod.* **11**, 891–897 (2005).
29. D. E. Cortezzo, B. Setlow, P. Setlow, *J. Appl. Microbiol.* **96**, 725–741 (2004).
30. E. Mancilla, E. Rojas, *FEBS Lett.* **260**, 105–108 (1990).
31. C. Mitchell, J. F. Skomurski, J. C. Vary, *FEMS Microbiol. Lett.* **34**, 211–214 (1986).
32. D. D. Lee *et al*., *Cell* **177**, 352–360.e13 (2019).
33. A. E. Cowan *et al*., *Proc. Natl. Acad. Sci. U.S.A.* **101**, 7733–7738 (2004).
34. A. Moir, D. A. Smith, *Annu. Rev. Microbiol.* **44**, 531–553 (1990).
35. A. P. Leonard *et al*., *Biochim. Biophys. Acta* **1853**, 348–360 (2015).
36. A. Perez-Valdespino *et al*., *J. Bacteriol.* **196**, 2077–2088 (2014).
37. K. Kikuchi *et al*., Electrochemical potential enables dormant spores to integrate environmental signals. Version 1, Zenodo (2022); https://doi.org/10.5281/zenodo.6967596.

ACKNOWLEDGMENTS

We acknowledge M. Asally, T. Çağatay, J. Larkin, C. Comerci, and K. Süel for helpful discussions; W. Winkler and D. Kearns for kindly providing bacterial strains; and J. Humphries for help with strain construction. **Funding:** National Institute of General Medical Sciences (grant R01 GM121888 to G.M.S.); National Institute of General Medical Sciences (grant R35 GM139645 to G.M.S.); Howard Hughes Medical Institute-Simons Foundation Faculty Scholars Program (G.M.S.); U.S. Army Research Office (W911NF2210107); Defense Advanced Research Projects Agency (HR0011-21-C-0192); Spanish Ministry of Science, Innovation and Universities (Project PGC2018-101251-B-I00 to J.G.O.); FEDER (CEX2018-000792-M to J.G.O.); Generalitat de Catalunya ICREA Academia program (J.G.O.); ANRI Fellowship (K.K.); and National Institute on Aging (grant RF1 AG062362 to E.A.T.). **Author contributions:** Conceptualization: K.K., L.G.L., C.W., J.G.O., and G.M.S.; Methodology: K.K., L.G.L., C.W., J.G.O., and G.M.S.; Experiments: L.G.L., K.K., and E.C.M.; Design, synthesis, and characterization of the charge-neutral version of ThT: J.Y.L. and E.A.T.; Experimental data analysis: K.K., L.G.L., and E.C.M.; Mathematical modeling: C.W. and J.G.O.; Funding acquisition: G.M.S., J.G.O., and E.A.T.; Supervision: G.M.S., J.G.O., and E.A.T.; Project administration: G.M.S.; Writing: G.M.S., K.K., L.G.L., C.W., J.G.O., E.C.M., J.Y.L., and E.A.T. **Competing interests:** The authors declare that they have no competing interests. **Data and materials availability:** All data are available in the manuscript or the supplementary material. All bacterial strains and material generated in this study are available from the authors. Code for the mathematical model and for generating the germination cumulative density functions are available at https://github.com/suellab/Kikuchi_Galera-Laporta_2022 and Zenodo (*37*). **License information:** Copyright © 2022 the authors, some rights reserved; exclusive licensee American Association for the Advancement of Science. No claim to original US government works. https://www.science.org/about/science-licenses-journal-article-reuse

SUPPLEMENTARY MATERIALS

science.org/doi/10.1126/science.abl7484
Materials and Methods
Supplementary Text
Figs. S1 to S10
References (*38*–*50*)
MDAR Reproducibility Checklist
Movies S1 to S4

Submitted 2 August 2021; resubmitted 9 February 2022
Accepted 9 August 2022
10.1126/science.abl7484

Downloaded from https://www.science.org at University of California San Diego on October 06, 2022

Science
AAAS

Supplementary Materials for

Electrochemical potential enables dormant spores to integrate environmental signals

Kaito Kikuchi, Leticia Galera-Laporta, Colleen Weatherwax, Jamie Y Lam, Eun Chae Moon, Emmanuel A Theodorakis, Jordi Garcia-Ojalvo, and Gürol M Süel
Correspondence to: gsuel@ucsd.edu

This PDF file includes:

Materials and Methods
Supplementary Text
Figs. S1 to S10
Tables S1 to S3
Captions for Movies S1 to S4

Other Supplementary Materials for this manuscript include the following:

Movies S1 to S4

Materials and Methods

Strains

All experiments were performed using the *Bacillus subtilis* strain NCIB 3610. The wild-type strain was a kind gift from W. Winkler (*38*) (University of Maryland). All strains used in this study can be found in Table S1. The *ΔktrC* and *ΔspoVAF* strains were made by PCR amplifying 1 kb regions upstream and downstream of the gene to be deleted and cloning them into the pER449 vector (gift from W. Winkler) and JDE131 vector, respectively, both flanking a spectinomycin resistance cassette. NEB turbo competent *E. coli* cells (New England Biolabs, Ipswich, MA, USA) were used for cloning purposes. Constructs were sequence verified and chromosomally integrated using a standard one-step transformation procedure (*39*). Luria Broth (LB) agar plates containing appropriate antibiotics were used to select *B. subtilis* transformants (spectinomycin, 100 μg ml^{-1}; neomycin 9 μg ml^{-1}; tetracycline 6 μg ml^{-1}). Primer sequences are described in Table S3.

Growth conditions

Sporulation was induced by resuspension medium (RM); composition per 1 L: 46 μg $FeCl_2$, 4.8 g $MgSO_4$, 12.6 mg $MnCl_2$, 535 mg NH_4Cl, 106 mg Na_2SO_4, 68 mg KH_2PO_4, 96.5 mg NH_4NO_3, 219 mg $CaCl_2$, 2 g monosodium L-glutamate (*40*). For RM without potassium used in Fig. S6, KH_2PO_4 was replaced with an equivalent amount of NaH_2PO_4. Germination was induced by 10 mM L-alanine, a condition typically employed in *Bacillus subtilis* germination studies (*41, 42*), or 100 mM L-valine. Monosodium L-glutamate and L-alanine solutions were made fresh weekly.

Preparation of spores with the Resuspension Method

Spores were prepared according to the Resuspension Method, known to promote sporulation in *B. subtilis* strain NCIB 3610 (*40*). A single *B. subtilis* colony was used to inoculate 5 mL of LB, and incubated overnight in a shaking incubator at 37 °C (200 rpm). The culture was diluted in 20% (v/v) LB at OD_{600} 0.1 and incubated at 37 °C with shaking until it reached OD_{600} 0.6 - 0.8. The culture was then centrifuged at 4,000 rpm for 10 min, resuspended in 1 volume of pre-warmed RM, transferred to a large vessel (250 mL Erlenmeyer flask for 50 mL culture) to ensure aeration, and incubated for three days at 37 °C in a shaking incubator (200 rpm).

The resulting spore suspension was washed with distilled water three times and suspended in 1 volume of distilled water. The spore suspension was stored at 4 °C.

Preparation of spores containing APG-4 AM and measuring APG-4 AM fluorescence

Asante Potassium Green-4 AM (APG-4; ION Biosciences, Texas, USA), a cell-permeant potassium fluorescence indicator dye, was used to measure the initial intracellular spore potassium concentration. Spores were prepared according to the method described above, with 2 μM APG-4 AM added to RM during the incubation time of three days. Spores were then washed and stored as described above. For fluorescence measurements, spores were placed in agar pads made from RM + 1.6% low-melting point agarose. Phase contrast and fluorescence snapshot images were taken with a Hamamatsu Orca-Flash4.0 LT+ camera under a 100X objective lens, using an Olympus IX83 inverted epifluorescence microscope. Single spores were segmented based on the phase-contrast image as described below in 'Single-spore tracking' and the resulting binary mask was used to measure APG-4 AM intensity for each spore. The resulting distributions were tested for statistical significance using the two-sample Kolmogorov-Smirnov test.

Calibration of the intracellular potassium indicator APG-4 AM

A single *B. subtilis* colony was used to inoculate 5 mL of LB, and incubated 2 h in a shaking incubator at 37 °C (200 rpm). 2 μM APG-4 AM was added to the culture and was further incubated for 45 min. Following the incubation, cells were washed with MSgg media (5 mM potassium phosphate (pH 7.0), 100 mM 3-(N-morpholino)propanesulfonic acid (pH 7.0), 2 mM $MgCl_2$, 700 μM $CaCl_2$, 50 μM $MnCl_2$, 100 μM $FeCl_3$, 1 μM $ZnCl_2$, 2 μM thiamine, 0.5% glycerol, 0.5% glutamate) and incubated for 1 h. 10 $\mu g.ml^{-1}$ valinomycin was added in the media for 1 h to equilibrate intracellular and extracellular potassium concentrations (*43*). Following this treatment, we loaded cells in four independent chambers of the microfluidic device and exposed them to the addition of different extracellular potassium concentrations (0, 100, 200, and 400 mM KCl), respectively, and inoculated 1 h to stabilize. Phase contrast and fluorescence snapshot images were taken and analyzed for each condition, as described above.

Microfluidic germination assay with germinant pulses

For microfluidic culturing, we used the CellASIC ONIX Microfluidic Platform and Y04D microfluidic plates (EMD Millipore). Prepared spore suspensions were loaded into the microfluidic chamber, and incubated for 1 h at 37 °C with RM supplied at 0.75 psi each from two wells for plate stabilization. After 1 h from the start of image acquisition, germinant pulses were delivered once every 2 h by switching to a well containing RM with 10 mM L-alanine for 3 min at 2.5 psi. After the germinant pulse, RM was supplied from two wells at 2.5 psi each to wash the chamber before returning to the baseline condition of 0.75 psi. The 3-minute pulse duration was selected based on the consideration of our 5-minute imaging rate, to allow sufficient time for germinant introduction and removal in the device.

Microfluidic germination assay with potassium channel blocker

For experiments using the potassium blocker quinine (Figs. 3 and 4), spores were prepared as usual and loaded into a microfluidic plate. 1 mM quinine (MilliporeSigma, St. Louis, MO, USA) was added to all wells containing RM, including the wells with 10 mM L-alanine. Before starting the experiment, spores were incubated in the presence of quinine at 37 °C for 45 min to ensure the efficacy of the drug. The germination assay was done according to the germinant pulse method described above.

Time-lapse microscopy

Spore germination was monitored with phase-contrast microscopy using an Olympus IX83 inverted epifluorescence microscope. Images were taken with an Orca-Flash 4.0 LT+ camera (Hamamatsu) and an X-Cite Turbo light source (Excelitas Technologies) under a 100X objective lens. Spore images were taken every 1 or 5 mins.

Dyes and concentrations

Electrochemical potential dynamics were measured using the fluorescent cationic dyes Thioflavin-T (ThT) or Tetramethylrhodamine, Methyl Ester, Perchlorate (TMRM), both at a concentration of 10 μM. The charge-neutral version of Thioflavin-T (neutral ThT) was used at a concentration of 10 μM. The extracellular potassium indicator APG-4 TMA and the intracellular potassium indicator APG-4 AM were used at a concentration of 2 μM.

Synthesis of charge-neutral ThT

The synthesis of neutral ThT was accomplished using a modification of a reported procedure (*43*). The spectroscopic and analytical data of the synthesized compound were identical to those reported in the literature (*45*). For the synthetic procedures and compound characterization see Fig. S9 and Supplementary Text.

Experimental Reproducibility

Data shown in the main figures were drawn from a minimum of three independent experiments. For multiple strains or conditions in the same panel, such as Figs. 2G and 3H, head-to-head experiments with WT spores (separate chambers in the same microfluidic device) were done on the same day as a control.

Single-spore tracking

Single spores were tracked using a combination of Fiji (https://imagej.nih.gov/ij/, RRID: SCR_002285) plugins. The stage drift in time-lapse phase-contrast images was corrected using the MultiStackReg plugin (http://bradbusse.net/sciencedownloads.html, RRID: SCR_016098). After drift correction, single dormant spores were segmented based on Otsu thresholding. Non-spore particles were discarded through size and shape filtering, and further manual inspection. The resulting binary mask was then used to measure the phase-contrast and fluorescence intensity of individual spores throughout the movie with the MultiMeasure plugin (https://www.optinav.info/Multi-Measure.htm).

Determination of germination time

Phase-contrast intensity data acquired through the previous step was analyzed by custom-written software in Python to calculate the germination time for each spore. Based on the well-known phase-contrast darkening that indicates spore rehydration during germination (*4*), we define germination time as the time where the phase-contrast intensity of the spore darkens beyond the background (Fig. S1A and B). Statistical analyses and data visualization were also performed by custom-written software in Python. Code used to detect germination has been deposited at the following GitHub repository: https://github.com/suellab/Kikuchi_Galera-Laporta_2022 (*37*).

Calculation of germination probability and integration capacity

The germination probability for each pulse was calculated by dividing the number of spores that germinated in response to the pulse, by the number of remaining dormant spores before the pulse. Integration capacity was defined as the average pairwise difference of concurrent germination probabilities, calculated up to the pulse of half-maximum germination. The half-maximum germination was determined from the corresponding dormant fraction curves.

Calculation of change in electrochemical potential

Change in electrochemical potential (Fig. 4F and G) was calculated for each spore by normalizing the ThT value for each spore with its initial ThT value. The average potential change (Fig. 4H) was obtained by extracting an average ThT value over a 20-minute window between each germinant pulse to establish the baseline of each step-wise increase. Then, the difference between each step was calculated to obtain the step sizes. Finally, the average step size across all the spores was obtained, up to the pulse were half of the population germinated (half-maximum germination).

Supplementary Text

Hodgkin-Huxley based potassium flux model

To describe the effect of potassium efflux on spore germination, we developed a Hodgkin-Huxley-based model of potassium flux in a dormant spore. We consider the germination event to be when the internal potassium concentration of the spore decreases below a certain threshold K_s. We assume that the initial potassium levels of a spore population follow a normal distribution.

Potassium ions can cross the spore membrane through ion channels. Potassium flux across the membrane depends on the fraction of ion channels that are open (n), the potassium ion concentration gradient, and the membrane potential of the spore (V), similar to a previously described model of potassium flux *(16)*. We explicitly modeled the dynamics of the intracellular and local extracellular potassium concentrations, K_i and K_e, respectively:

$$\frac{dK_e}{dt} = Fg_K n^4(V - V_K) + Fg_n n^4(V - V_n) - \gamma_e(K_e - K_m) \tag{1}$$

$$\frac{dK_i}{dt} = -Fg_K n^4(V - V_K) - Fg_n n^4(V - V_n) \tag{2}$$

Potassium can enter and leave the spore through both dedicated potassium channels and nonspecific ion channels. The first term in both equations describes potassium flux through potassium ion channels, and the second term describes potassium flux through nonspecific ion channels. The nonspecific ion Nernst potential is approximated by the parameter V_n, and the potassium Nernst potential V_K is given by the equation:

$$V_K = V_{K0} \ln (K_e/K_i) \tag{3}$$

The dynamics of the spore's membrane potential is described by the following ordinary differential equation:

$$\frac{dV}{dt} = -g_K n^4 (V - V_K) - g_n n^4 (V - V_n) \tag{4}$$

The ion channels are assumed to effectively have four subunits, which can be in an open or closed position. The fraction of subunits n that are in the open position is described by the following equation, where the first term represents the opening of the channels due to germinant exposure and the second term represents their closing:

$$\frac{dn}{dt} = \alpha(1 - n) - \beta n \tag{5}$$

When germinant is not present, $\alpha = 0$; otherwise, $\alpha = \alpha_g$. As a consequence, in the absence of germinant, the entire system is at steady state with channels closed, reflecting the idea that spores are dormant and stable.

Modeling genetic and chemical perturbations

We assume that cells lacking KtrC are less able to actively transport potassium into the cell than wild-type cells. Therefore, we assumed that Δ*ktrC* spores have lower average intracellular potassium levels than wild-type spores. Consequently, the starting membrane potential for Δ*ktrC* spores is more negative than for wild-type spores.

Cells lacking the YugO channel have a potassium channel conductance of 0, or $g_K = 0$. Potassium ions can only enter or leave the Δ*yugO* spore through the nonspecific ion channels, which have a much lower conductance for potassium, so potassium efflux is slower than in wild-type spores. In addition, Δ*yugO* spores have less intracellular potassium than wild-type spores, and correspondingly a slightly more negative membrane potential. Finally, we assume that Δ*yugO* cells are less able to regulate potassium levels before and during sporulation, thus causing the distribution of initial intracellular potassium levels to be more variable than those of wild-type cells.

Quinine is assumed to decrease channel conductance, to g_{Kq} and g_{nq} for potassium channels and nonspecific ion channels, respectively.

Scheme and procedures for the synthesis of neutral ThT

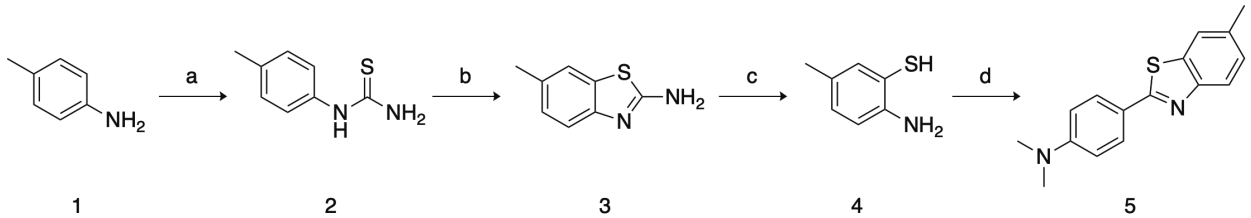

Scheme 1. *Reactions and conditions for the synthesis of Neutral ThT.* (a) 1.0 equiv **1**, 1.1 eq NH_4SCN, 27% aq. H_2SO_4, 20 h, 85 °C, 61%; (b) 1.0 equiv **2**, 0.1 equiv HBr, conc. H_2SO_4, 2 h, 80 °C, 57%; (c) 1.0 equiv **3**, 40% NaOH, 20h, 100 °C, 31%; (d) 1.0 equiv *p*-dimethylaminobenzaldehyde, 1.2 equiv **4**, cat. amberlite IR-120, EtOH, mw irradiation, 3 h, 100°C, 40%.

1-(p-tolyl)thiourea (2) *(46)***:** To an aqueous solution of H_2SO_4 (27%, 10.0 mL) was added in one portion commercially available p-toluidine (**1**) (5.00 g, 46.66 mmol, 1.0 equiv.) and ammonium thiocyanate (3.91 g, 51.33 mmol, 1.1 equiv.). The reaction was allowed to stir overnight at 85 °C. Upon completion (tlc monitoring), toluene (10.0 mL) was added and the reaction mixture was refluxed for 1h. The solution was neutralized with NH_4OH and filtered to yield compound **2** as a white solid (61% yield). R_f = 0.35 (1:9 EtOAc:DCM); ^{1}H NMR (300 MHz, $CDCl_3$): δ 7.87 (bs, 1H), 7.24 (d, J = 8.2 Hz, 2H), 7.12 (d, J = 8.3 Hz, 2H), 6.03 (bs, 2H), 2.37 (s, 3H). *(47)*

6-methylbenzo[d]thiazol-2-amine (3) *(46)***:** To a solution of **2** (2.00 g, 12.03 mmol, 1.0 equiv.) in conc. H_2SO_4 (4.0 mL) was added slowly 48% HBr (0.08 mL, 1.20 mmol, 0.1 equiv.). The reaction was allowed to stir at 80 °C for 2 h. The reaction was diluted with cold water, neutralized with NH_4OH and extracted with EtOAc (3 x 15.0 mL) to afford **3** as a pale-yellow solid (57% yield). R_f = 0.10 (1:9 EtOAc:DCM); ^{1}H NMR (300 MHz, $CDCl_3$): δ 7.44 (d, J = 8.19, 1H), 7.41-7.40 (m, 1H), 7.12 (dq, J = 8.2, 0.6 Hz, 1H), 5.07 (bs, 2H), 2.40 (s, 3H).

2-amino-5-methylbenzenethiol (4) *(48)***:** To a solution of 40% NaOH (12.5 mL) was added **3** (1.00 g, 6.09 mmol, 1.0 equiv.) and the reaction was heated at 100 °C for 20h. Upon completion (tlc monitoring), the solution was neutralized with AcOH then filtered to yield compound **4** as an off-white solid (31% yield). R_f = 0.75 (100% EtOAc); ^{1}H NMR (300 MHz, $CDCl_3$): δ 6.99-6.95 (m, 2H), 6.64 (d, J = 7.9 Hz, 1H), 4.18 (s, 2H), 2.13 (s, 3H) *(49)*.

N,N-dimethyl-4-(6-methylbenzo[d]thiazol-2-yl)aniline (Neutral ThT, 5) *(50)***:** To a 5.0 mL microwave vial was added *p*-dimethylamino benzaldehyde (0.05 g, 0.34 mmol, 1.0 equiv.) and **4** (0.05 g, 0.40 mmol, 1.2 equiv.) in EtOH (3.0 mL). A few beads of Amberlite IR-120 were added, and the reaction was subjected to microwave radiation at 100 °C for 3h. The precipitate was collected via filtration to provide **5** as a pale yellow solid (40% yield); R_f = 0.85 (1:9 EtOAc:DCM); ^{1}H NMR (500 MHz, $CDCl_3$): δ 7.94 (d, J = 8.9 Hz, 2H), 7.86 (d, J = 8.3 Hz, 1H), 7.63 (s, 1H), 6.25 (dd, J = 0.8, 8.6 Hz, 1H), 6.74 (d, J = 8.9 Hz, 2H), 3.05 (s, 6H), 2.47 (s, 3H); ^{13}C NMR (125 MHz, $CDCl_3$): δ: 167.95, 152.54, 152.14, 134.75, 134.35, 128.82, 127.62, 121.87, 121.60, 121.33, 111.80, 40.33, 21.63; HRMS (ESI-TOF) calculated for $[C_{16}H_{17}N_2S]^+$ $[M+H]^+$: 269.1107; found 269.1106 *(45)*.

Fig. S1.

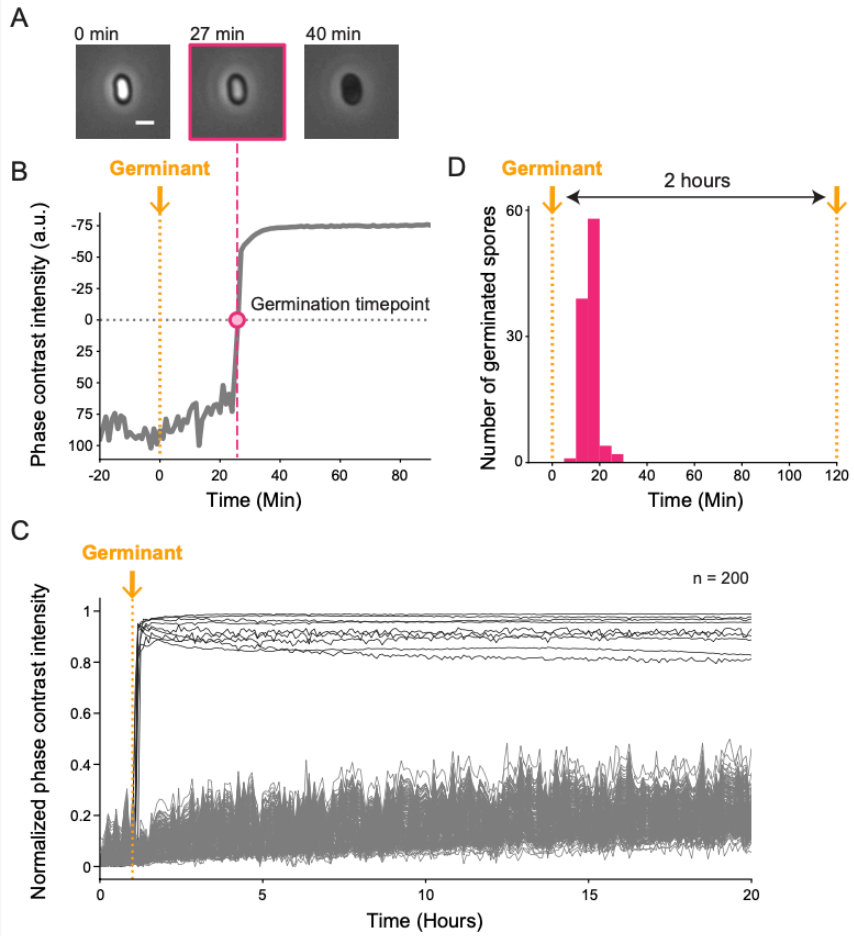

Germination dynamics of spores in response to a single germinant pulse.
(A) Filmstrip of a representative germinating wild-type (WT) spore. The snapshot bordered in magenta corresponds to the timepoint where the spore is considered to have germinated (germination timepoint). Scale bar indicates 1 µm.
(B) Corresponding single-cell time trace of the spore in panel A showing phase-contrast intensity (a.u.). After subtracting the background signal, the germination timepoint (magenta circle) is detected as the timepoint where the phase contrast intensity becomes negative (darkens beyond background level). The 3-minute pulse of germinant (10 mM L-alanine) is indicated with a dotted vertical line.
(C) Normalized phase-contrast intensity time traces of WT spores exposed to a single germinant pulse (n = 200). Notice that changes in camera focus create global changes of phase-contrast values.
(D) Histogram of germination timepoints in response to a single 3-minute germinant pulse (14.68 ± 0.66 minutes, n = 104). Data from Fig. 1D.

Fig. S2.

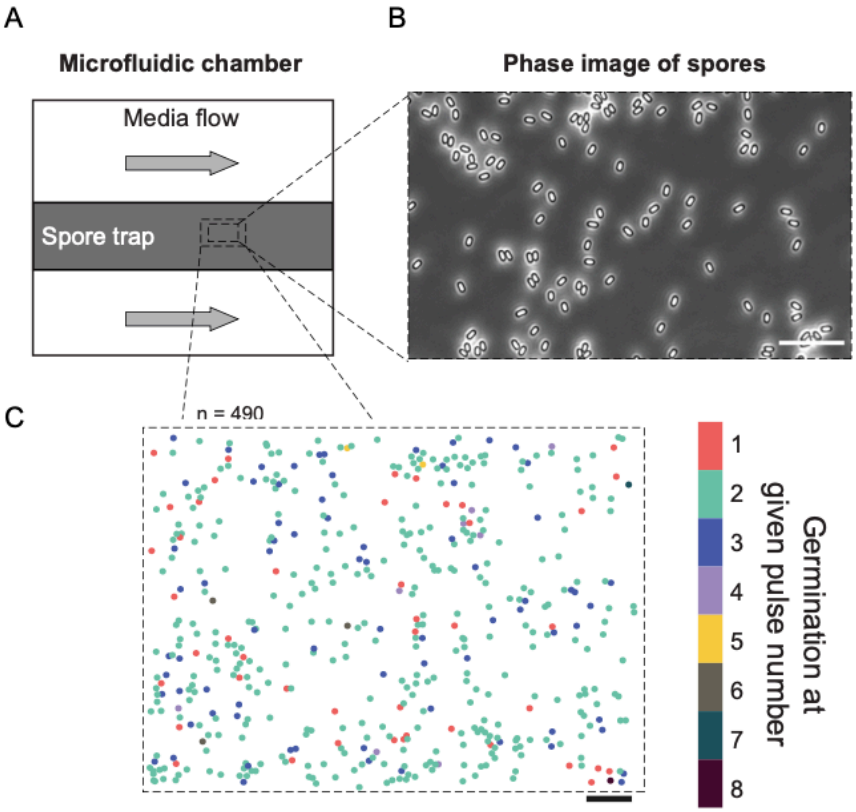

Germination does not correlate with spatial position within the microfluidic chamber.
(A) Cartoon illustrating the microfluidic chamber used in this study. Spores are trapped in a chamber with media flow on each side.
(B) A representative snapshot of WT spores in the spore trap. Scale bar indicates 10 µm.
(C) Plot showing WT spores in their respective locations within the spore trap. Colors correspond to the germinant pulse number in which they germinated. Scale bar indicates 10 µm.

Fig. S3.

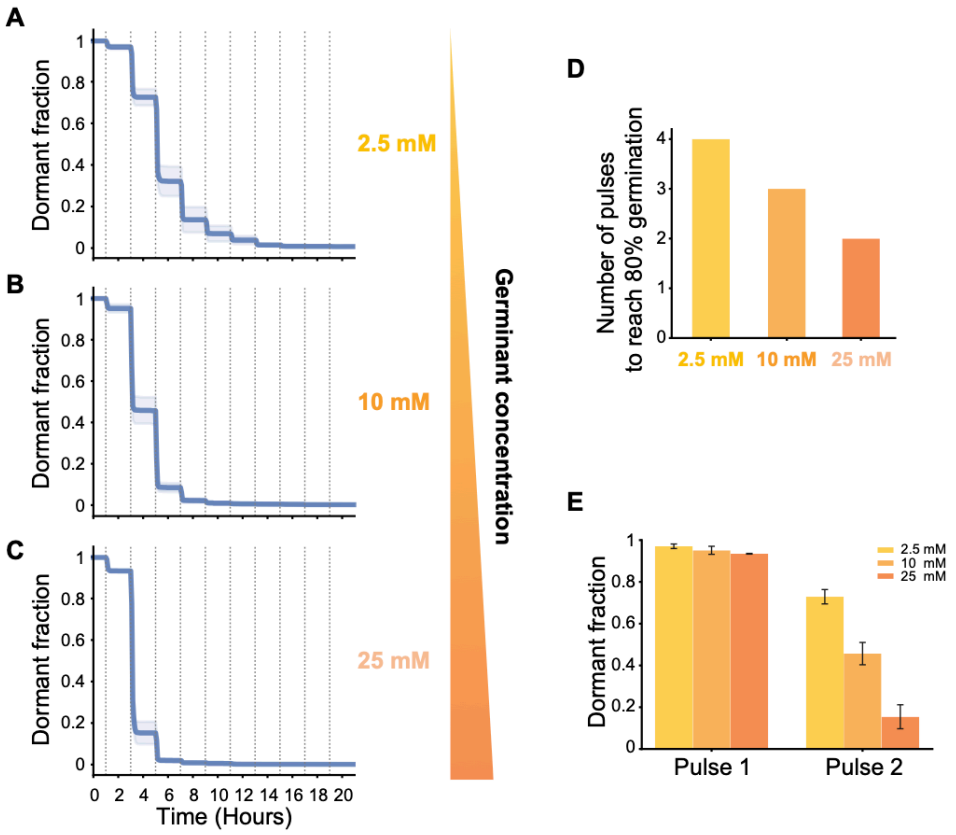

The sensitivity of spores to different germinant concentrations support the integrate-and-fire model.

(A-C) Dormant fraction cumulative distribution functions (CDFs) of WT spores subjected to pulses of 2.5, 10, and 25 mM L-alanine (2.5 mM, n = 3,794; 10 mM, n = 2,244, data from Figure 2G; 25 mM, n = 2,668). For all cases, the interval between pulses is 2 h.

(D) The bar plot indicates the number of germinant pulses required to reach 80% germination. Data from panels A-C.

(E) The bar plot indicates the dormant fraction for each condition after the 1st and 2nd pulses. Data from panels A-C. Error bars represent standard deviation.

Fig. S4.

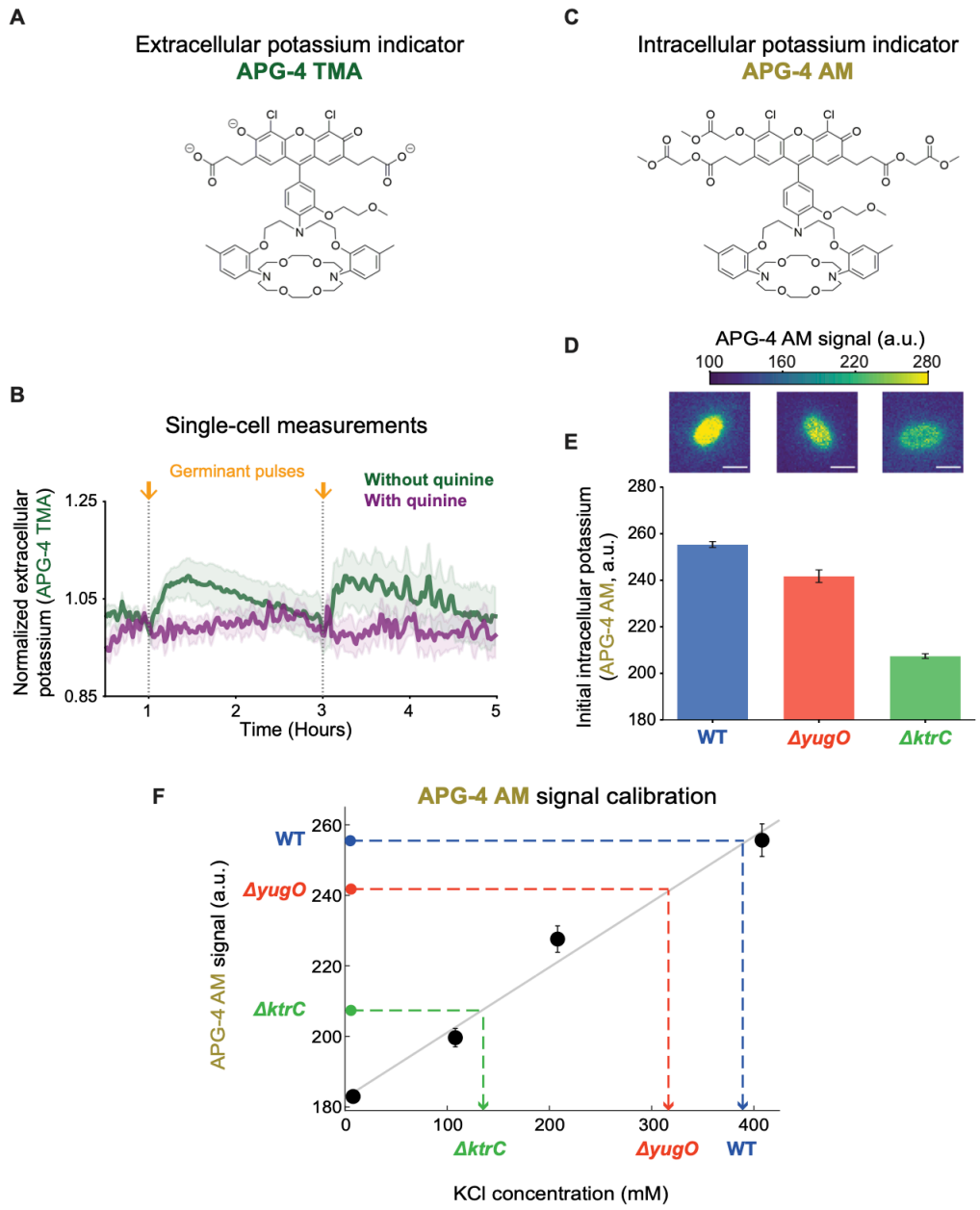

Potassium measurements in dormant spores using fluorescent indicators.
(A) Structure of the extracellular potassium indicator APG-4 TMA.
(B) Average fluorescent time traces from single WT spores stained with 2 µM of the extracellular potassium indicator APG-4 TMA, without (green, n = 20) or with 1 mM quinine addition (purple, n = 24). The 3-minutes pulse of germinant (10 mM L-alanine) is indicated with vertical dotted lines. Shaded regions represent standard deviation. Data was normalized to 1 at the 1-hour mark. All spores remained dormant during the timescale shown in the plot.
(C) Structure of the intracellular potassium indicator APG-4 AM.

(D) Representative fluorescence snapshots of WT, *ΔyugO*, and *ΔktrC* spores stained with the intracellular potassium indicator APG-4 AM. Scale bars indicate 1 µm.
(E) Average fluorescence intensities of dormant WT (blue, n=1,037), *ΔyugO* (red, n=776), and *ΔktrC* (green, n=1,107) spores that were generated in the presence of 2 µM APG-4 AM. Both *ΔyugO* and *ΔktrC* intensities were significantly lower compared to WT ($p<1*10^{-14}$, two sample Kolmogorov-Smirnov test). Error bars indicate standard error of the mean.
(F) Calibration curve for the intracellular potassium fluorescence indicator APG-4 AM. The black data points indicate APG-4 AM measurements for cells exposed to the addition of different KCl concentrations (0, 100, 200, and 400 mM KCl). Error bars indicate standard deviation. The mean values for dormant WT, *ΔyugO*, and *ΔktrC* spores are indicated with the dotted lines (data from panel D).

Fig. S5.

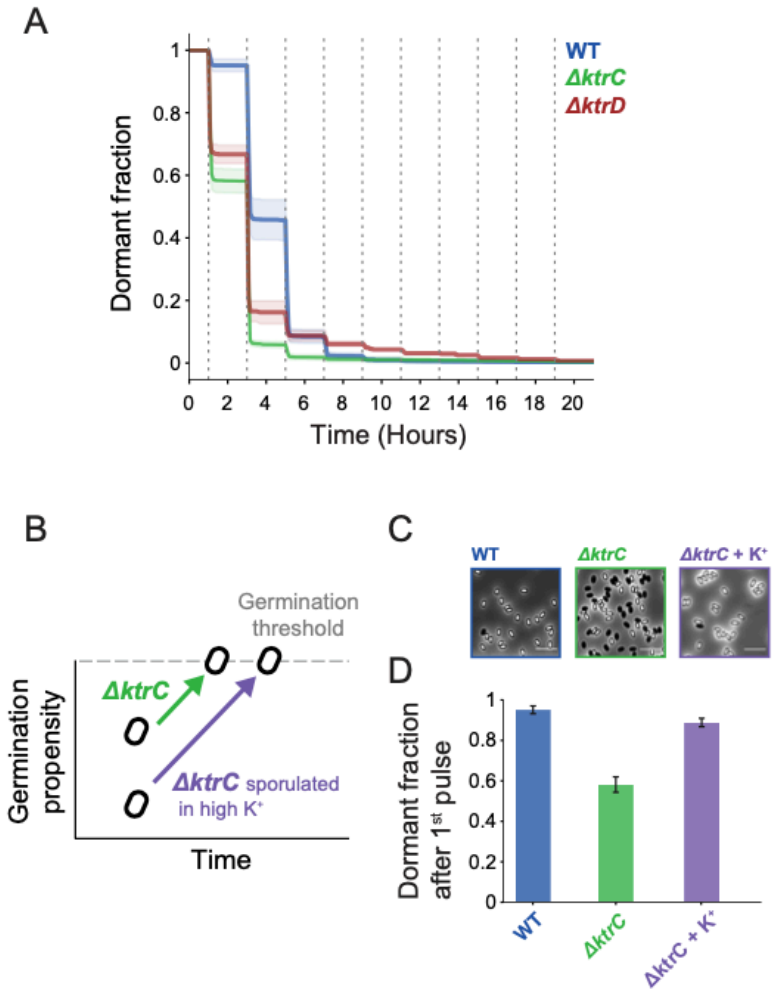

Rescue of the *ΔktrC* phenotype confirms that intracellular potassium levels determine the distance to the germination threshold.
(A) Dormant fraction for single-cell experiment results for WT (blue, mean ± SD, n = 2,244, data from Fig. 1D), *ΔktrC* (green, mean ± SD, n = 2,154, data from Fig. 3G), and *ΔktrD* (brown, mean ± SD, n = 442). The dotted vertical lines indicate timepoints where 3-minute pulses of 10 mM L-alanine were applied.
(B) Cartoon illustrating that higher potassium concentration in the sporulation medium increases the distance of *ΔktrC* spores to the germination threshold, rescuing the *ΔktrC* phenotype.
(C) Snapshots for representative WT, *ΔktrC*, and *ΔktrC* spores with 150 mM potassium addition during sporulation. Snapshots show spores after the 1st germinant pulse. Scale bars indicate 5 µm.

Fig. S6.

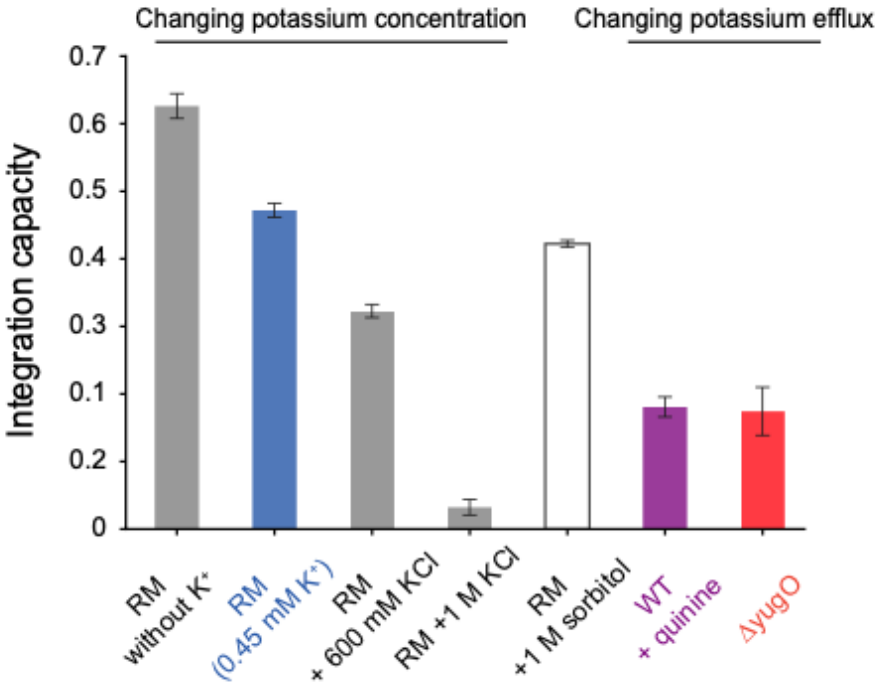

Modulation of potassium efflux recapitulates *ΔyugO* phenotype.
Integration capacities of WT spores (n = 2,244, data from Fig. 1D), WT spores in various external KCl concentrations (RM without K^+, n = 903; 600 mM, n = 1,061; 1 M, n = 1,699), WT spores in presence of 1 M sorbitol (n = 2,819), WT spores in presence of 1 mM quinine (n = 4491, data from Fig. 3J), and *ΔyugO* spores (n = 1,058, data from Fig. 3J). Error bars indicate standard deviation.

Fig. S7.

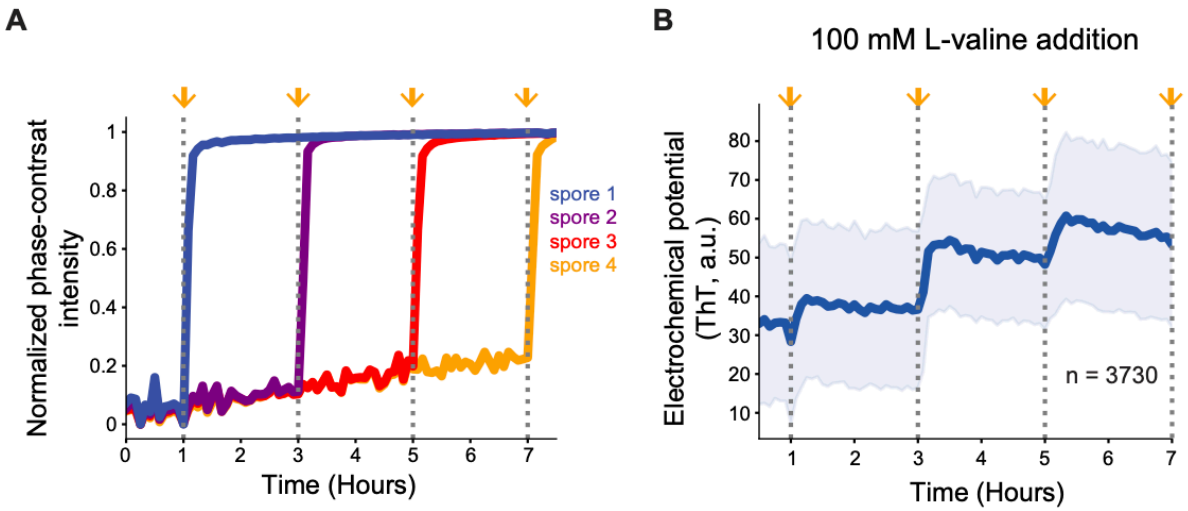

Phase contrast of spores during germinant pulses and ThT dynamics in response to L-valine pulses.
(A) Single-cell time traces of min-max normalized phase-contrast intensity for spores shown in Fig. 4D and E. Notice that changes in camera focus create global changes of phase-contrast values. The dotted vertical lines indicate timepoints where 3-minute pulses of 10 mM L-alanine were applied.
(B) Mean fluorescence time trace of WT spores stained with 10 µM ThT (mean ± SD, n = 3,730). The dotted vertical lines indicate timepoints where 3-minute pulses of 100 mM L-valine were applied. The shaded area corresponds to the standard deviation.

Fig. S8.

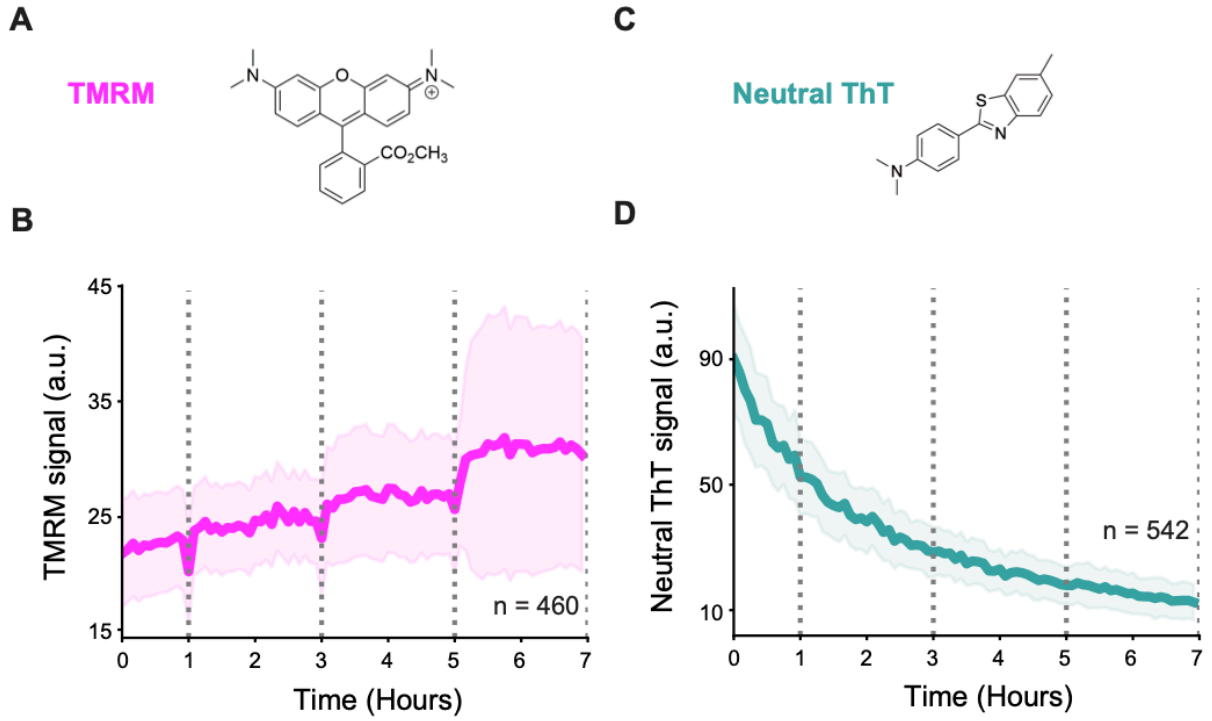

Comparison of charged and uncharged electrochemical potential reporter dyes.
(A) Chemical structure of the cationic fluorescent dye Tetramethylrhodamine methyl ester (TMRM).
(B) Mean fluorescence time trace of WT spores stained with 10 µM TMRM (mean ± SD, n = 460). The mean is calculated from fluorescence values before each spore's germination timepoint. The shaded area corresponds to standard deviation.
(C) Chemical structure of the charge-neutral ThT.
(D) Mean fluorescence time trace of WT spores stained with 10 µM neutral ThT (mean ± SD, n = 542). The mean for all germinated spores shows a decrease in signal likely due to photobleaching. The shaded area corresponds to standard deviation.

Fig. S9.

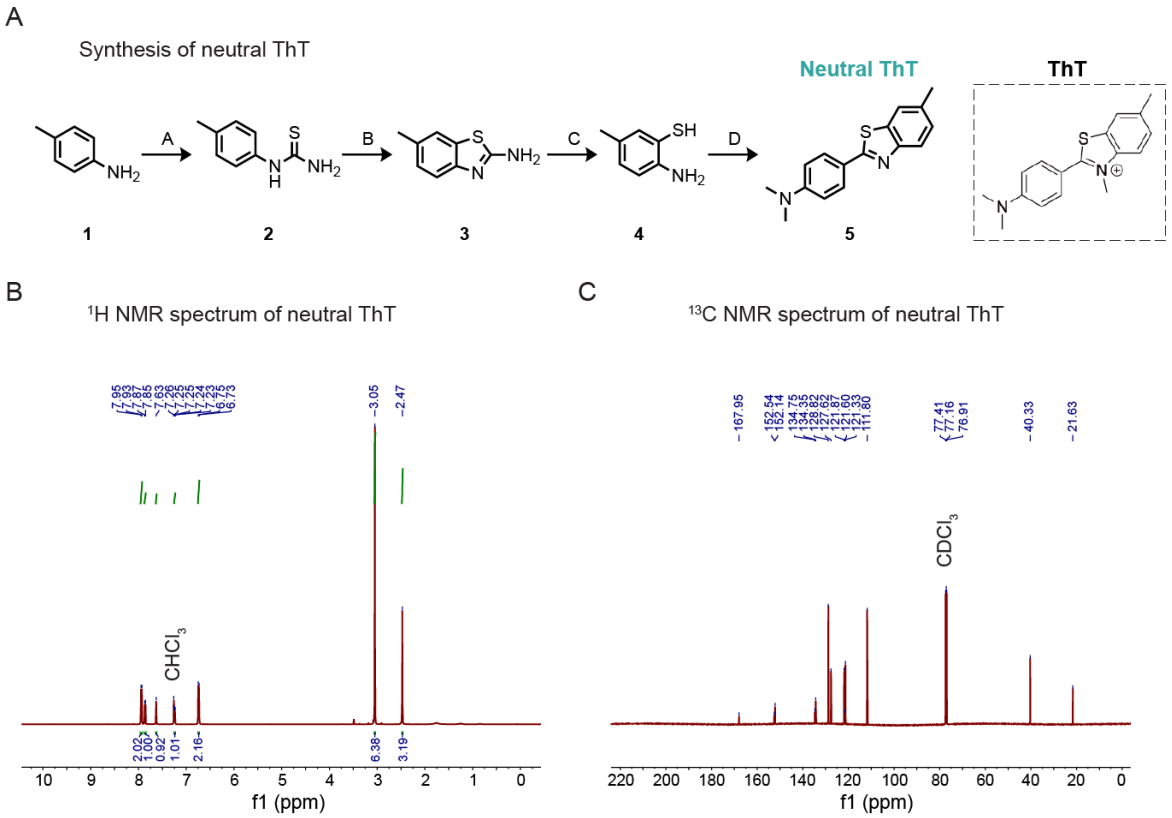

Synthesis and characterization of neutral ThT.
(A) Intermediates for the synthesis of neutral ThT: (1) p-toluidine, (2) 1-(p-tolyl)thiourea, (3) 6-methylbenzo[d]thiazol-2-amine, (4) 2-amino-5-methylbenzenethiol, (5) N,N-dimethyl-4-(6-methylbenzo[d]thiazol-2-yl)aniline ("neutral ThT"). Reactions and conditions: (A) 1.0 equiv 1, 1.1 eq NH_4SCN, 27% aq. H_2SO_4, 20h, 85 °C, 61%; (B) 1.0 equiv 2, 0.1 equiv HBr, conc. H_2SO_4, 2 h, 80 °C, 57%; (C) 1.0 equiv 3, 40% NaOH, 20h, 100 °C, 31%; (D) 1.0 equiv p-dimethylaminobenzaldehyde, 1.2 equiv 4, cat. amberlite IR-120, EtOH, mw irradiation, 3h, 100 °C, 40%.
(B) ^{1}H Nuclear Magnetic Resonance (NMR) spectrum of neutral ThT. The observed signals correspond to the protons in neutral ThT and are used to confirm the chemical structure. Green lines represent the integration (number of protons corresponding to each signal, annotated under the peaks). The signal for the solvent ($CHCl_3$) is at 7.26 ppm.
(C) ^{13}C NMR spectrum of neutral ThT. The observed signals correspond to the carbons in neutral ThT and are used to confirm the chemical structure. The signal for the solvent ($CDCl_3$) is at 77.41, 77.16, and 76.91 ppm.

Fig. S10.

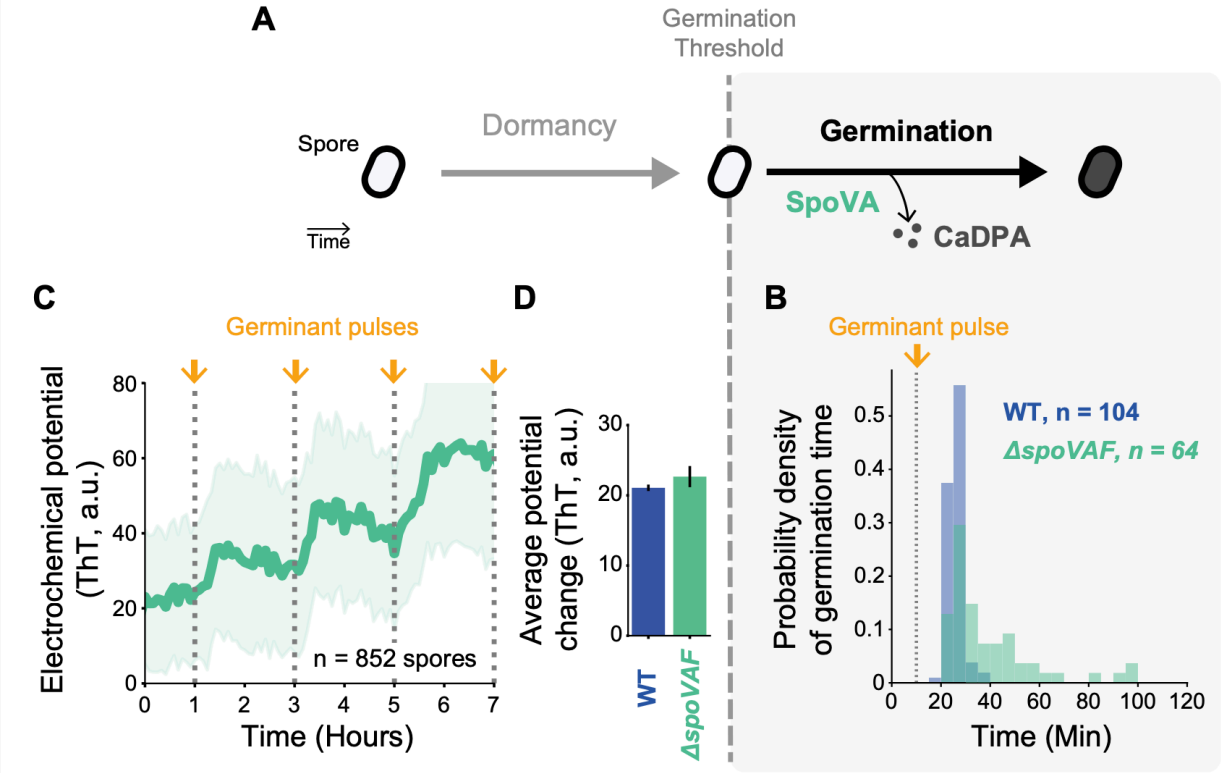

Deletion of the SpoVAF subunit of the SpoVA CaDPA channel does not affect electrochemical dynamics in dormant spores.
(A) Cartoon illustrating the efflux of CaDPA through the SpoVA channel, a well-known process in the germination process following germination triggering.
(B) Normalized histogram of germination timepoint probability densities in response to a single 3-minute germinant pulse; WT (n = 104, data from Fig. 1D and S1D) and *ΔspoVAF* (n = 64).
(C) Mean fluorescence time trace of dormant *ΔspoVAF* spores stained with 10 µM ThT (n = 852). The dotted vertical lines indicate 3-min pulses of 10 mM L-alanine. The shaded area corresponds to standard deviation.
(D) Bar plots indicating average electrochemical potential change of WT (n = 3,484, data from Fig 4F) and *ΔspoVAF* (n = 852, data from panel C) spores. Error bars represent 99% confidence intervals.

Table S1.

Strain	Genotype	Source
Wild type	*B. subtilis* NCIB 3610	Gift from Wade Winkler laboratory (University of Maryland, College Park, MD) *(38)*
ΔyugO	*yugO::* neo	Laboratory collection *(16)*
ΔktrC	*ktrC::* spec	This study
ΔktrD	*ktrD::* tet	Gift from Daniel Kearns laboratory (Indiana University Bloomington, IN)
ΔspoVAF	*spoVAF::* spec	This study

Strains used in this study.

Table S2.

Parameter	Description	Value	Units
g_K	potassium channel conductance	30	min^{-1}
g_{Kq}	potassium channel conductance (with quinine)	1	min^{-1}
g_n	nonspecific channel conductance	0.08	min^{-1}
g_{nq}	nonspecific channel conductance (with quinine)	0.005	min^{-1}
V_{K0}	Nernst potential prefactor	30	mV
V_n	nonspecific ion Nernst potential	-130	mV
α_g	channel opening constant due to germinant	3	min^{-1}
β	channel opening rate decay constant	0.6	min^{-1}
$V_{0\text{WT}}$	initial membrane potential (wild-type)	-79	mV
$V_{0\text{ktrC}}$	initial membrane potential ($\Delta ktrC$)	-81	mV
$V_{0\text{yugO}}$	initial membrane potential ($\Delta yugO$)	-80	mV
γ_e	extracellular potassium relaxation rate	1	min^{-1}
F	membrane capacitance	5.6	mM/mV
K_m	external media potassium	8	mM
K_s	potassium threshold triggering germination	235	mM
K_{WT}	average initial potassium concentration (wild-type)	300	mM
K_{ktrC}	average initial potassium concentration ($\Delta ktrC$)	275	mM
K_{yugO}	average initial potassium concentration ($\Delta yugO$)	280	mM
σ_{WT}	st. dev. of initial potassium concentration (wild-type)	15	mM
σ_{ktrC}	st. dev. of initial potassium concentration ($\Delta ktrC$)	15	mM
σ_{yugO}	st. dev. of initial potassium concentration ($\Delta yugO$)	35	mM

Modeling parameters for potassium-efflux model.

Table S3.

Strain	Name	Sequence
ΔktrC	ktrC-5' arm F	AACTCGCTTCTGTTTGTATACGGGAC
	ktrC-5' arm R	CTATGACCATGATTACGCCAAGCTGGAAGTTTGTTTGCTGCAAAAGAGGG
	ktrC-3' arm F	TGGCTTAACTATGCGGCATCAGAGGCTTGAGATCGGCAGCTTTGAG
	ktrC-3' arm R	CCTGCCACACGGGCATCAAG
ΔspoVAF	spoVAF-5' arm F	CCGGCGCAAATGCAGACAATATCAGCACGGATTTATCGGAATCGGCATGG
	spoVAF-5' arm R	TTAGCTGGATTCCGATAAACCCGAATTTTC
	spoVAF-3' arm F	TCACGAACGAAAATCGCCATTCGCCGGCAGCCTACCAATTCATAATCGCA
	spoVAF-3' arm R	GCGTATCACGAGGCCCTTTCGTCTTTCAAAGATTTGCGAGCCGATATGGC
	Spectinomycin resistance F	CGGGTTTATCGGAATCCAGCTAAGATGATCCCCCTATGCAAGGGTTTATTC
	Spectinomycin resistance R	GGCGAATGGCGATTTTCGTTCG
	JDE131 vector F	AAGACGAAAGGGCCTCGTGATACG
	JDE131 vector R	CTGATATTGTCTGCATTTGCGCCG

Primer sequences for strains constructed in this study.

Movie S1
Phase-contrast time lapse movies for WT (top left) and *ΔktrC* spores (bottom left). The scalebar indicates 5 μm. The corresponding plot on the right shows individual germination events over time, indicated by lines transitioning from gray to black. In all panels, orange flashes and lines indicate 3-minute germinant pulses.

Movie S2
Phase-contrast time lapse movies for WT (top left) and *ΔyugO* spores (bottom left). The scalebar indicates 5 μm. The corresponding plot on the right shows individual germination events over time, indicated by lines transitioning from gray to black. In all panels, orange flashes and lines indicate 3-minute germinant pulses.

Movie S3
Phase-contrast time lapse movies for WT spores either in the absence (top left) or presence (bottom left) of 1 mM quinine in the germinant pulse. The scalebar indicates 5 μm. The corresponding plot on the right shows individual germination events over time, indicated by lines transitioning from gray to black. In all panels, orange flashes and lines indicate 3-minute germinant pulses.

Movie S4
Time lapse movies for WT spores stained with ThT (top row), arranged from left to right in the order in which they germinate. Corresponding phase-contrast movies are shown as an inset. The scalebars indicate 1 μm. The timing for germination is indicated by the top label 'Exit.' The potential change for each spore is plotted below with corresponding colors. In all panels, orange flashes and lines indicate 3-minute germinant pulses.